FINAL REPORT

ALPHA FOUNDATION FOR THE IMPROVEMENT OF MINE SAFETY AND HEALTH

Final Technical Report

Project Title: Low noise efficient rim driven auxiliary ventilation fans

Grant Number: AFC215-21

Organization:	Virginia Polytechnic Institute and State University (Virginia Tech)
	Mechanical Engineering Department
	445 Goodwin Hall
	635 Prices Fork Road - MC 0238
	Blacksburg, VA 24061

Principal Investigator: Prof. Ricardo A. Burdisso
Contact Information : Email Address: rburdiss@vt.edu
Phone Number: 540-231-7355

Co-Principal Investigator: Prof. Pablo A. Tarazaga
Contact Information : Email Address : ptarazag@vt.edu
Phone Number: 540- 231-2906

Administrative Contact: Jane Lee, MBA, CRA
Contact Information : Email Address : janelee@vt.edu
Phone Number: 540-231-6653

Period of Performance: September 2015-December 2017

Table of Contents

1. Executive Summary:

According to NIOSH, noise is one of the greatest hazards to a miner's health, rivaled only by respirable dust and repetitive trauma (Matetic et al., 2012). The exposure to harmful noise levels reduces work efficiency, causes accidents, and causes noise induced hearing loss from prolong exposure (Xiang Hua et al., 2012). Consequently, there is still a pressing need to reduce the exposure of high noise levels in the working areas. One of the most harmful sources of noise is temporarily mounted auxiliary ventilation fans. They are used to maintain a safe level of oxygen, dilute and remove noxious gases, control airborne dust, and control temperature and humidity in the working areas. Temporarily mounted auxiliary ventilation fans are particularly detrimental to the physical and mental health due to their close proximity to the workforce. This problem exists because most ventilation fans (if not all) are not really designed with quiet operation in mind or even aerodynamic considerations. In fact, the main driver in the design/fabrication of these fans is to lower cost. Some examples of the reason current industrial fans are loud are: the fan blades are not aerodynamically shaped (e.g. flat plates of constant chord), the inlet duct has sharp lip edges that can result in flow distortion ingested by the fan, large blade tip gap, and so forth.

Therefore, there are opportunities to significantly reduce the noise from these auxiliary fans by proper design and implementation of the latest noise control technologies. Consequently, the main aim of this project was to experimentally demonstrate a novel quiet portable ventilation fan that will improve the mining environment and reduce noise and induced hearing loss of the workers.

A key premise of this research is that a fan with a very low tip speed with an optimum blade design is the best approach to reduce noise. This is because noise typically scales to the 4-6th power of the fan tip speed. Therefore, the trend in the design of fans has been to reduce the fan speed while increasing the fan diameter to maintain the volumetric flow rate. However, floor space restrictions in working areas can significantly restrict the fan diameter (Lawrence Berkeley National Laboratory, 1989). Consequently, a compact low speed fan can significantly contribute to the improvement of the health and safety of mine workers by providing a high volumetric flow rate and low noise levels in a constrained work environment.

As part of this research effort, a new quiet fan was designed, fabricated and tested to demonstrate that it is possible to design a compact, low tip speed, quiet fan with high volumetric flow rate. This new fan is shown in Figure 1 and referred here as the VTQR fan. In the same figure, the sound power level in dBA and volumetric flow rate in CFM of the VTQR fan (green data point) is compared to data collected from commercial fans obtained from published manufactured data, e.g. data was assumed accurate. The comparison shows that only a few commercial fans (inside the shaded area in the plot) are quieter and generate more CFM than the VTQR fan. The fan diameter for these fans is also indicated in the figure. It is noticeable that all of these fans have diameters that are between 25% and 100% larger than the VTQR fan, i.e. 0.45 to 0.71 m versus 0.362 m for the VTQR fan.

Consequently, this effort significantly contributes to the improvement of the health of mine workers by reducing their exposure to high noise levels, i.e. preventing hearing loss. Additionally, this work has shown that it is possible to reduce noise levels by 15-20 dB relative to typical commercial fan system by incorporating effective noise control technologies.

VTQR Fan – 0.362 m (14.25") diameter
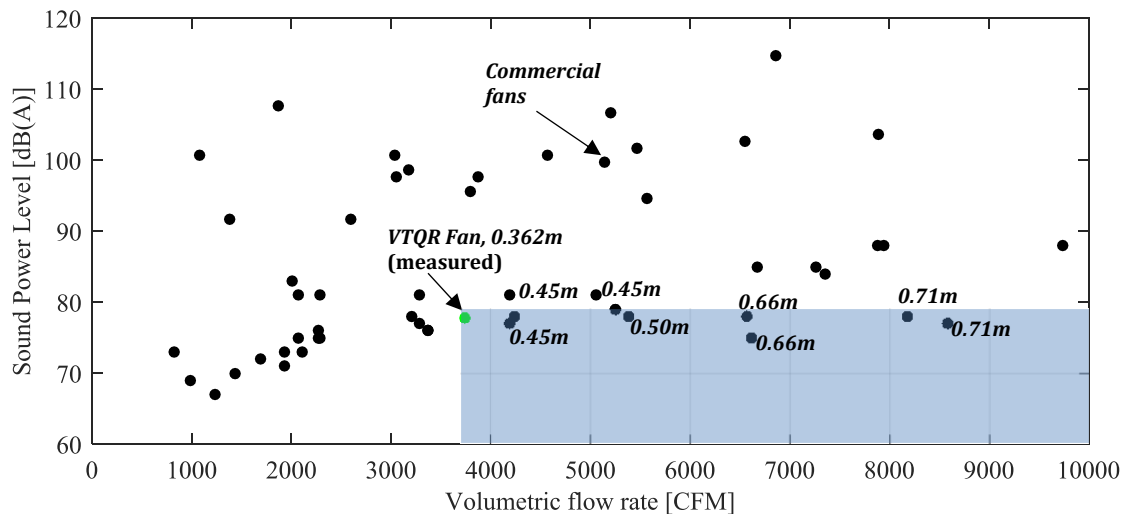
Figure 1: VTQR fan comparison to commercial ventilation fans.

2. Problem Statement and Objective:

2.1 Problem Statement

Physical hazardous agents that mine workers are exposed to on a daily basis include among others noise, vibration, temperature, and dust. Noise--induced hearing loss is a critical issue for the mine workforce. According to NIOSH noise is one of the greatest hazards to a miner's health, rivaled only by respirable dust and repetitive trauma (Matetic et al., 2012). Thus, there is still a pressing need to reduce the exposure of miners to noise. If the Permissible Exposure Level (PEL) is exceeded, the mine operator is required to use all feasible engineering and/or administrative controls to reduce miner's exposure. This is not a trivial problem as there are several noise sources in a mining operation that can contribute to this challenge. Ventilation fans are one of the most dominant noise sources and thus a prime target for noise control and mitigation. In fact, ventilation fans are the second loudest noise source in coal mine operations (Cherniack et al., 2012). Ventilation systems must provide air to all places in an underground mine to maintain a safe level of oxygen, dilute and remove noxious gases, control airborne dust, and control temperature and humidity in the working areas. The primary ventilation system for underground mines consists of a very large surface fan pumping air and distributing it through the mine. Temporarily mounted auxiliary ventilation fans are also used to supplement the air to specific working areas. These fans are much smaller than the primary one. However, these auxiliary fans are in close proximity to the miners and thus have a more detrimental impact on the workers. This ventilation fan noise problem is not unique to the mine operations, and is very common through many other industries.

2.2 Problem Objectives

The main aim of this project is to experimentally demonstrate a novel quiet portable ventilation fan that will improve the mining environment by preventing noise induced hearing loss of the workers. The novel quiet fan makes use of technologies developed for other applications, primarily in the defense and aeronautic fields. To this end, the main objectives of the project were:

1. To optimally design a new fan incorporating the most effective noise controls technologies.
2. To fabricate a prototype fan system for experimentally demonstrating the target 15-20 dB noise reduction while maintaining/improving aerodynamic performance and electrical power consumption.

3. Research Approach:

The main premise of this research effort was that a fan with a very low tip speed with an optimum blade design is the best approach to reduce noise. This is because the noise typically scales to the 4-6th power of the fan tip speed. Therefore, reducing the fan speed will reduce the noise levels significantly. The second premise to reduce noise was to implement a rim driven fan to eliminate many of the noise sources present in typical fans. To this end, the research approach has been to divide the effort into two phases. In phase I, a small-scale fan demonstrator (0.134 m diameter) was used to provide an efficient approach to demonstrate and establish the benefits of the proposed technologies: lowering the fan tip speed and rim driven fan. In phase II, a quiet realistic fan (0.362 m diameter) was optimally designed to minimize noise using the lessons learned from the Phase I work. In addition, the performance of the quiet realistic fan was compared to commercial ventilation fans. For the sake of clarity and consciences, the new quiet realistic fan designed will be referred by the acronym VTQR (**V**irginia **T**ech **Q**uiet **R**ealistic). Figure 2 shows the test fans designed, fabricated and tested in the two phases of the project. The four setups developed in Phase I are either rim driven (rigs 1 and 2) or rim mounted (rigs 3 and 4). The two setups in Phase II are rim mounted and free-tip configurations. In the free-tip case, the fan is mounted to the hub and it is the approach used by all commercial fans. These experimental setups and the lessons learned from their testing are described in the next subsections.

(a) Phase I: Subscale Fans

(b) Phase II: VTQR Fan

Test rig 1

Rim-mounted

0.134 m

0.362 m

Test rig 2

Free-tip

Test rig 3

Test rig 4
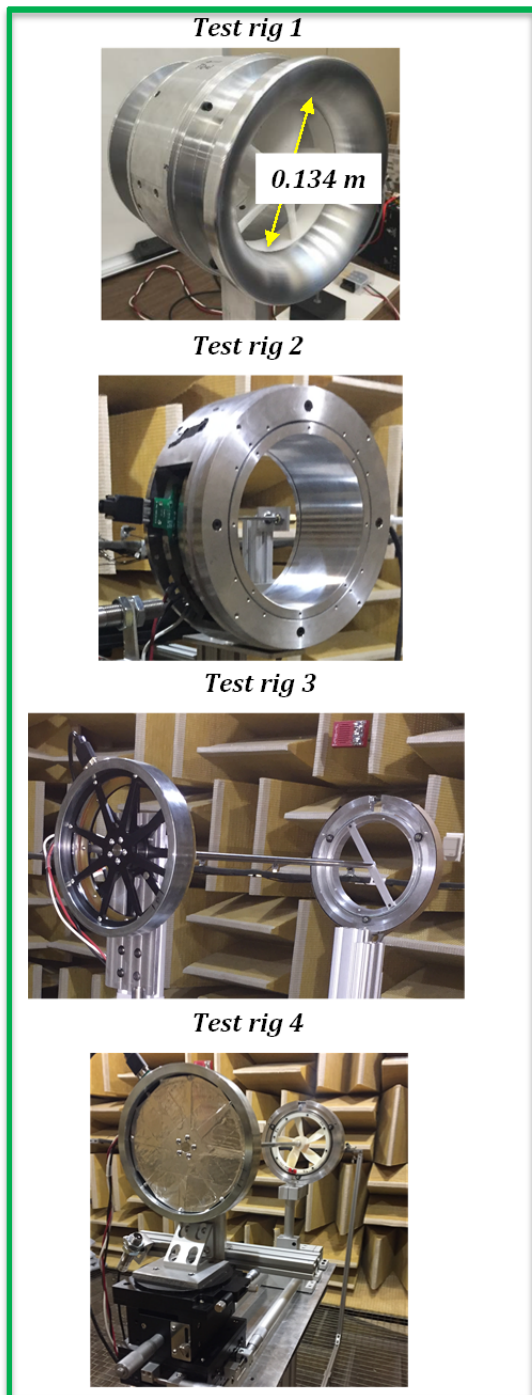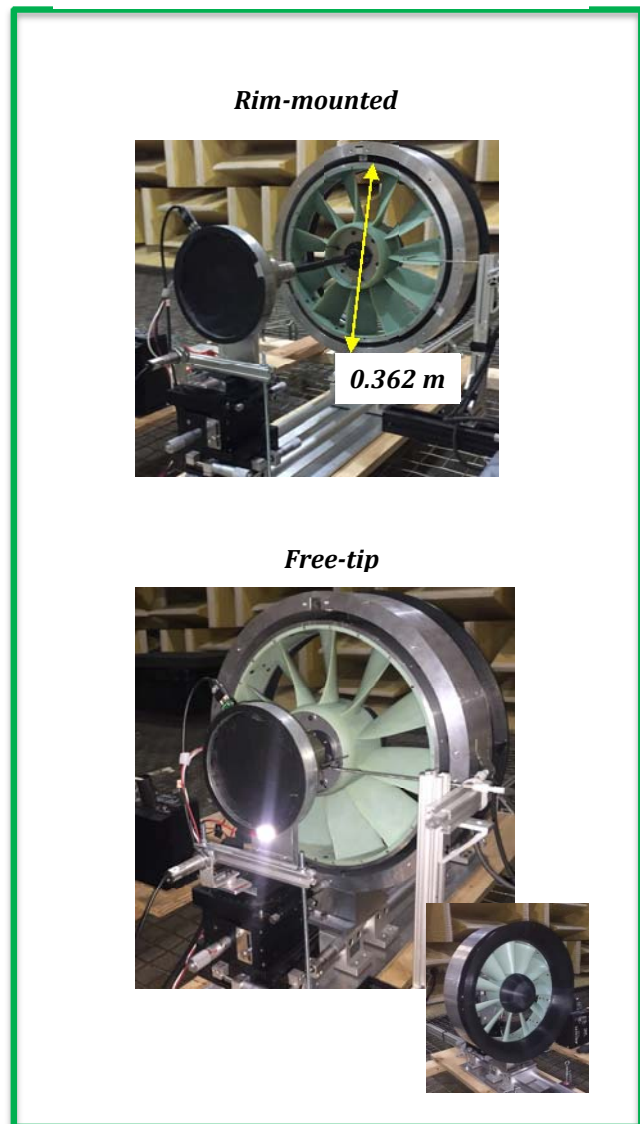
Figure 2: Fans tested in the phase I and II of the project.

3.1 Phase I: Small scale Fan demonstrator

In the Phase I, the fans were designed using the conventional free-vortex design approach, e.g. generate uniform velocity and pressure over the entire rotor area. From an extensive trade study, two fans were designed that met the project objectives. The two fans were fabricated using 3D printing technology and implemented using a DC Brushless motor. The motor selected for driving the fans was the ThinGap DC Brushless motor. The motor selection process is presented in Appendix A. This motor was selected because it allowed testing of the fans up to 8100 RPM and generated up to 4.52 N-m (3.33 lbf-ft) of torque, well past the required fans power and torque. The motor and fans were integrated using two approaches: a rim-driven and a rim-mounted approach.

3.1.1 Fan design

The fan design process consisted of identifying the design targets, conducting a trade study, and analyzing the effects of the duct. A description of all of the aerodynamic and acoustic codes used for the design and analysis of the fans is presented in Appendix B.

3.1.1.1 Design targets

The design targets of the small scale fan demonstrator have been guided by carefully analyzing and gauging the current state-of-the-art of commercially available fans. To this end, data from 80 axial commercial ventilation fans with diameters ranging from 0.180 to 0.8 m was collected from various well-known manufacturers. The data includes fan diameter, number of blades, speed (revolution per minute or rpm), volumetric flow rate (in cubic feet per minute or cfm), and sound pressure/power level (if available in the datasheets). The specifications of the commercial ventilation fans are presented in Appendix C. To identify targets for the design of the small scaled fans, data for the commercial ventilation fans was normalized to account for fans of different sizes. The key fan parameters that were normalized are:

- The volumetric flow rate (cfm) was normalized by the fan area resulting in the exit flow velocity.
- The fan speed was normalized by the fan diameter resulting in the fan tip velocity, typically expressed in Mach.
- The sound pressure level reported at a given distance was used to estimate the sound power level and then normalized by the fan diameter to obtain the sound intensity level produce by the fans, which is independent of distance and fan diameter.

The commercial ventilation fan normalized data was used to identify the target fan tip Mach number, exit flow velocity, and sound intensity level for the design of the small scale fan demonstrator. The normalized data for the commercial ventilation fans in the form of exit flow velocity vs fan tip speed and sound power level vs fan tip speed is plotted in Figure 3 and Figure 4, respectively. The design targets are shown as a shaded area in these figures. Specifically, the targets for the design of the small fan demonstrator were:

i.   Design fan speed range was selected to be: 0.14 to 0.2 Mach
ii. Fan axial flow velocity target range was: 15 to 25 m/s, and
iii. Fan sound power level should be reduced by 15-20 dB relative to the average sound power level trend shown in Figure 4.

Therefore, the aim of the design of the small scale fan is to reduce the sound intensity level by 15-20dB while operating in the target tip Mach number and exit flow velocity range illustrated by the blue box target region in Figure 3 and Figure 4.
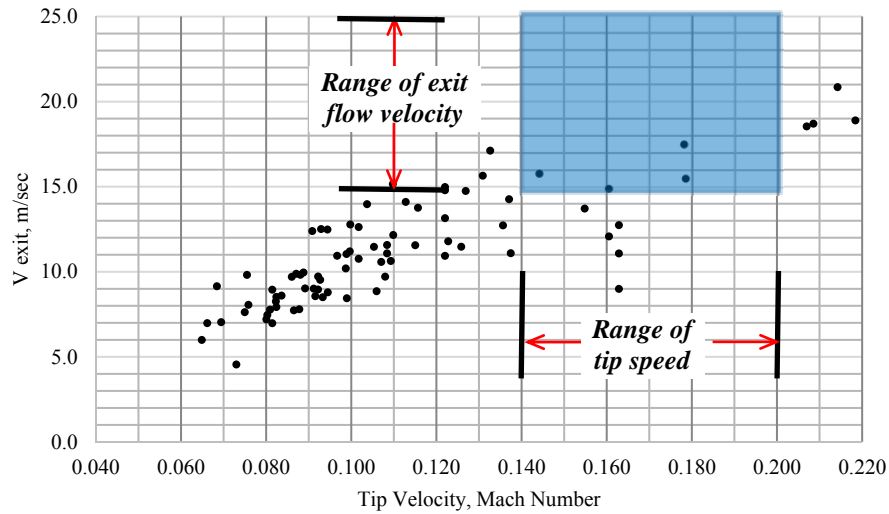
Figure 3: Exit flow velocity vs fan tip speed (Mach) for commercial fans and target tip Mach and exit flow velocity range for small scale fan demonstrator.
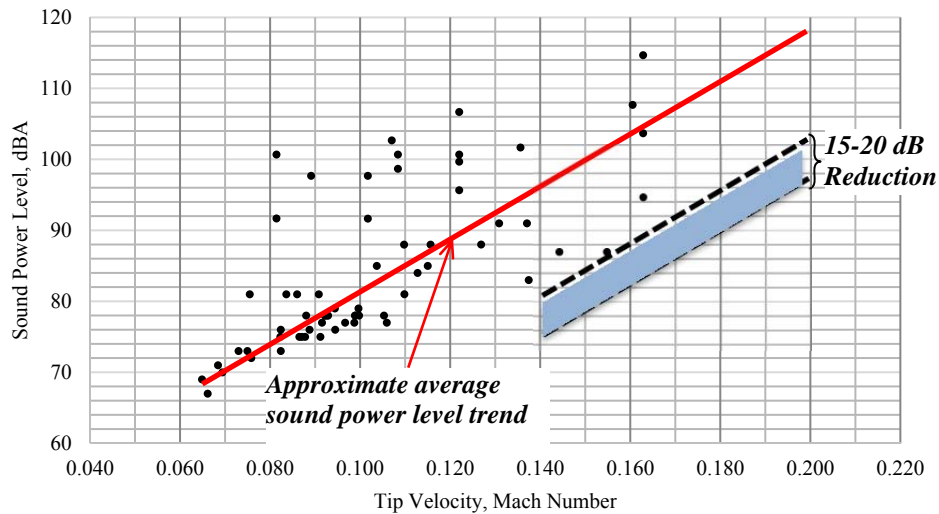
Figure 4: Sound power level vs fan tip speed (Mach) for commercial fans and target sound power level for small scale fan demonstrator.

3.1.1.2   Fan Blade design

In phase I, the fans were designed using the free-vortex design methodology. The two important characteristics of the free vortex design methodology are:

- The blade geometry is narrow at the tip and widen toward the hub due to the decrease in the blade tangential velocity towards the hub (tangential velocity is assumed to be inversely proportional to the radius)
- The twist angle of the blades is maximum at the hub and monotonically decreases towards the tip. This allows for a uniform velocity and pressure over the entire rotor area.

The design process involved several steps. The first step was to apply constraints related to the design targets (Section 3.1.1.1). Then, geometrical constraints for the fan based on the ThinGap motor were implemented. The next step was to identify the airfoils to use that would result in the highest efficiency (minimum drag). To that end, an airfoil dimensionless analysis methodology (Hurtado et al., 2017) was developed and published under the conference proceeding of NOISE-CON 2017 Noise Control: Improving the Quality of Life. The dimensionless analysis approach allowed identifying the E214-PT airfoil and the DF101 airfoils as the best two airfoils to use in the design process. The geometry characteristics of the two airfoils are presented in Table 1.

Table 1: Airfoils considered in the fan design.

Airfoil name	Thickness (%)	Camber (%)	Airfoil geometry
E214A-PT	11.1	4	
DF101-PT	11	2.3	

Using these airfoils, a trade study (aerodynamic and acoustic) was performed. A total of 473 fans were designed for the target range of exit flow velocities and tip Mach numbers. All the fans designed had evenly spaced fan blades. From the 473 fans the best two fans were selected by analyzing the geometry, noise, and aerodynamic results for each case. The main geometric constrains for the best designs were the following:

  i.   a blade twist of less than 85 degrees at the hub,
 ii.   a blade chord at the hub less than 75% of the radius, and
iii.   a blade chord at the tip greater than 1.5 cm.

The two selected designs were referred as fans 171 and 349. The performance and geometric parameters for these two fans are presented in Table 2 and Table 3, respectively. Figure 5 shows isometric and side views of the fans. The main difference between these fans is the number of blades. Fan 171 has 5 blades while fan 349 has 7 blades. Another less obvious difference is that the chord distribution is more uniform for the fan 349. Both fans have the same design speed of 6400 RPM (0.16 tip Mach number).

The power, torque, volumetric flow rate and sound power level have been evaluated for an RPM range of 1000 to 7000 and they are plotted in Figure 6. As shown here, the power consumption of fan 171 is slightly lower and produces less noise (1.5 dB). Figure 6c also shows the noise target of 73.8 dBA, e.g. fan demonstrator noise should be below this line for a minimum noise reduction of 15 dB relative to the trendline for commercial ventilation fans. However, it is important to note that the noise produced by the motor and the bearings is not included in the results Figure 6c. Instead, they were directly measured.

Table 2: Key performance parameters for fan designs selected for testing.

Run number	Axial Flow (m/s)	Volumetric flow rate (CFM)	Design Tip Mach number	Noise (dBA)	Mechanical Power at Design (Watts)	Torque (N-m)
171	20	799	0.16	62.8	103	0.15
349	20	799	0.16	64.3	105	0.16

Table 3: Key geometric parameters fan designs selected for testing.

Geometry					
Case	Chord Hub (cm)	Chord Tip (cm)	Twist Hub (deg.)	Twist Tip (deg.)	Num. blades
171	5.5	2.1	77	24	5
349	4.5	2.6	77	23	7

Design case	Isometric view	Side view
171		
349		
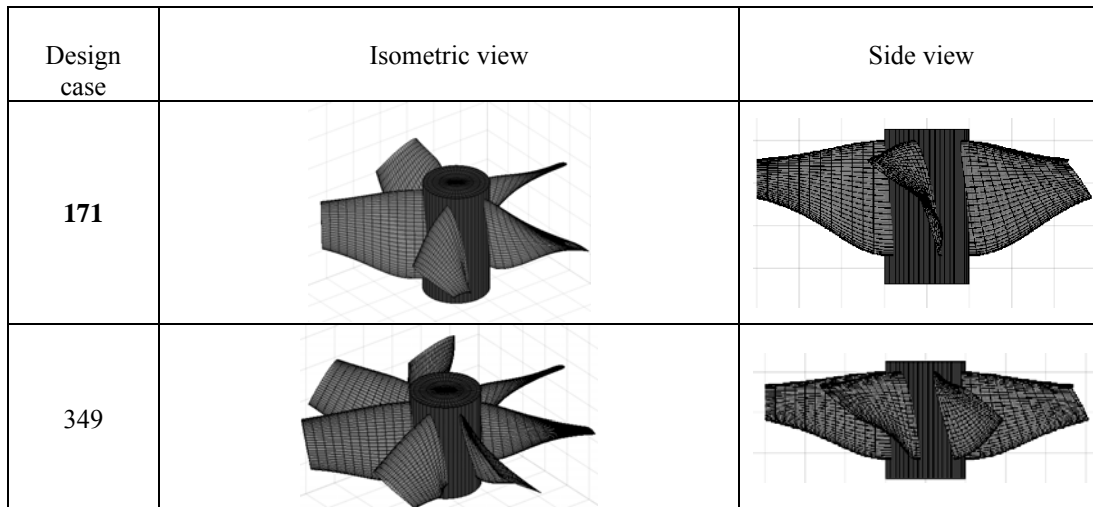
Figure 5: Isometric and side views of fan designs selected for testing.
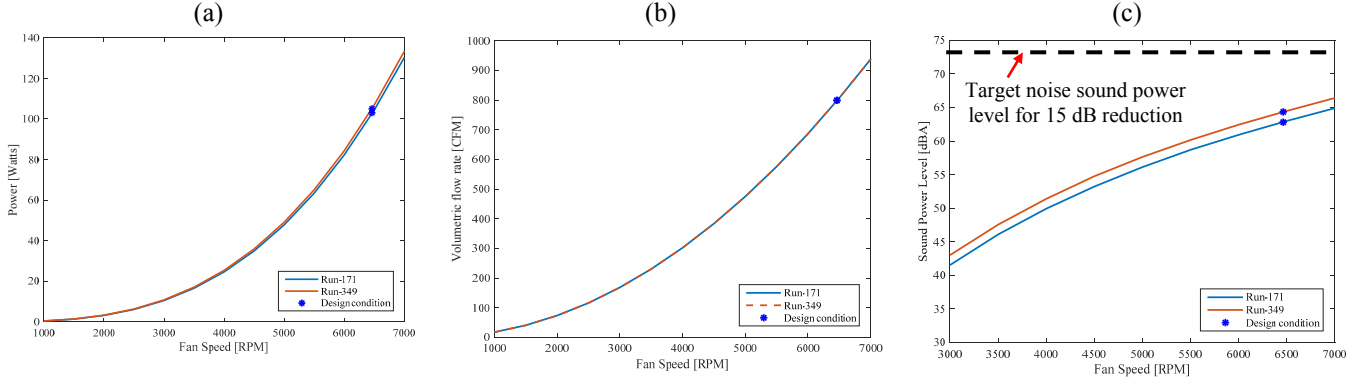
Figure 6: (a) Mechanical power vs fan speed, (b) CFM vs fan speed, and (c) Sound Power Level vs fan speed for fan 171 and 349.

3.1.1.3 Fan Inlet duct and Hub

The next step was to design a bell mouth inlet and a cone hub. The effect of the bell mouth and cone hub on the fan aerodynamic performance was estimated using the code DFDC. The geometry of the hub, duct and rotor is shown in Figure 7. Here, the flow velocity at the fan face is the most important result and it is shown in Figure 8. In the design of the fan (section 0), the fan generated a uniform flow on the fan plane (free-vortex design) as shown in Figure 8 (blue line). However, the effect of the inlet and hub is a non-uniform higher flow velocity distribution (red line). The axial velocity is nearly uniform, ranging from 21.6 m/s at the hub to 22.8 m/s at duct wall. The non-uniform velocity distribution is due to the duct induced thrust which was not accounted for in the initial design. Though not perfectly uniform, it is very close to the uniform velocity of 20 *m/s* (blue line). In summary, the design of the duct and hub was satisfactory since it generates a nearly uniform velocity distribution as sought. Additionally, the duct design provided a higher volumetric flow rate, e.g. average flow velocity of 22.2 m/s.
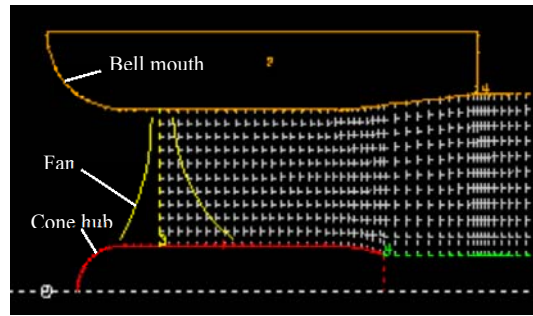

Figure 7: Inlet and hub geometry.

13
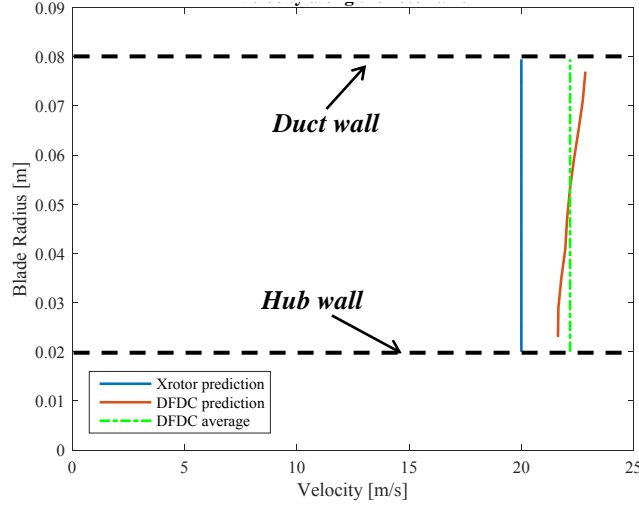
Figure 8: Axial flow velocity distribution along radial direction (fan plane).

3.1.2   Fan fabrication

The fans were constructed using a CONNEX 3 OBJET500 3D printer at Virginia Tech. The material used for the fabrication of the fans was the high temperature RGD525 material manufactured by Stratasys. The RGD525 material was chosen because it has excellent dimensional stability and one of the highest tensile strengths available at 70-80 MPa (10,000-11,500 psi). Figure 9 shows the 3D printed prototype fans 171 and 349.

(a)   (b)
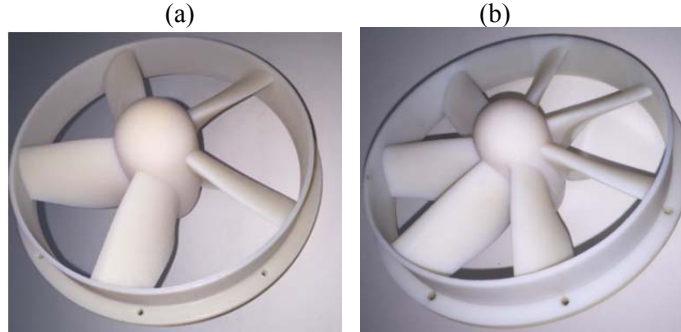
Figure 9: 3D printed fans (a) 171 and (b) 349.

3.1.3   Fan demonstrators

The fan demonstrators built to test fan 171 and 349 are presented in this section. Two different approaches were used for testing the fans: rim driven and rim mounted. The rim mounted approach was designed to address high noise level issues with the rim driven approach and the higher than expected electrical power consumption. This section presents a description of the four test rigs shown in Figure 2a.

Rim driven fan – Rig 1

The rim driven fan demonstrator was designed to incorporate the ThinGap TG7140 motor with no modifications to the motor. The mounting system uses two large commercially available Kaydon bearings (PN: KA060CP0, speed limit: 2500 rpm) face clamped on the bearing housing. Figure 10 shows the bearings used which have a bore diameter 6.0" with a 0.25" cross section. This commercial off the shelf ball bearings was selected due to its stability and availability. None of the conventional ball

bearings available with large bore diameter have a speed limit higher than 6000 RPM at its design load. However, it is possible to operate a bearing over its speed limit under light loads. Since the load for the prototype fans is less than 1% of the bearing load limits, it was advised by the manufacturer engineers that it was not an issue to operate the bearings above the 6000 RPM limit. Figure 11 shows how the ThinGap TG7140 motor, two Kaydon bearings, and fan fit together using an exploded view of the disassembled hardware components. The machining and fabrication of the mounting hardware was performed in the Mechanical Engineering Department machine shop of Virginia Tech. Figure 12a shows the CAD generated geometry of the rig 1 small scale. Figure 12b shows the assembled demonstrator. Except for the fan, all the parts were machined from 6061 aluminum.

(a)   (b)

**Figure 10:** Kaydon thin-section beairng, Part number: KA060CP0, (a) Top view (b) Side view.
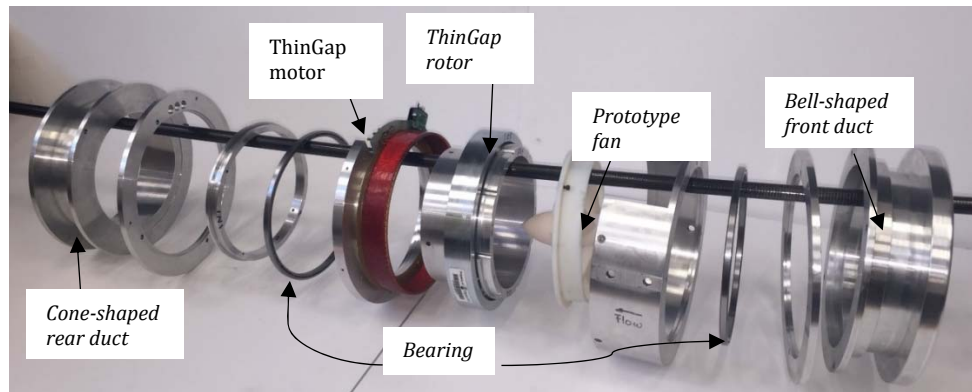
Figure 11: Pictures of small fan demonstrator components disassembled.
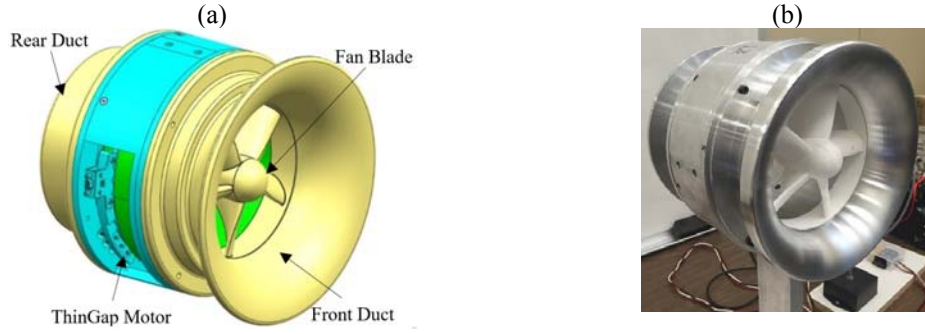
Figure 12: Rig 1 small scale prototype fan (a) isometric view of the CAD geometry and (b) fabricated and assembled hardware.

Rim driven fan – Rig 2

The main problem with rig 1 was the excessive noise and electrical power consumption due to the large bearings. The electrical power was twice the power required to operate the fan. Therefore, in rig 2, an array of four miniature bearings were used to replace the large Kaydon bearings to reduce noise and electrical power. Figure 13a shows rig 2using a CAD exploded view. The final assembled and fabricated rig is shown in Figure 13b. The miniature bearings are commercially available, low cost, and capable of very high speeds. The bearings are expected to operate around ~80k rpm as the fan reaches the target fan speed of 4000 rpm. Two type of miniature bearings were used as listed in Table 4. Actual photo of these miniature bearings are also shown in the table.
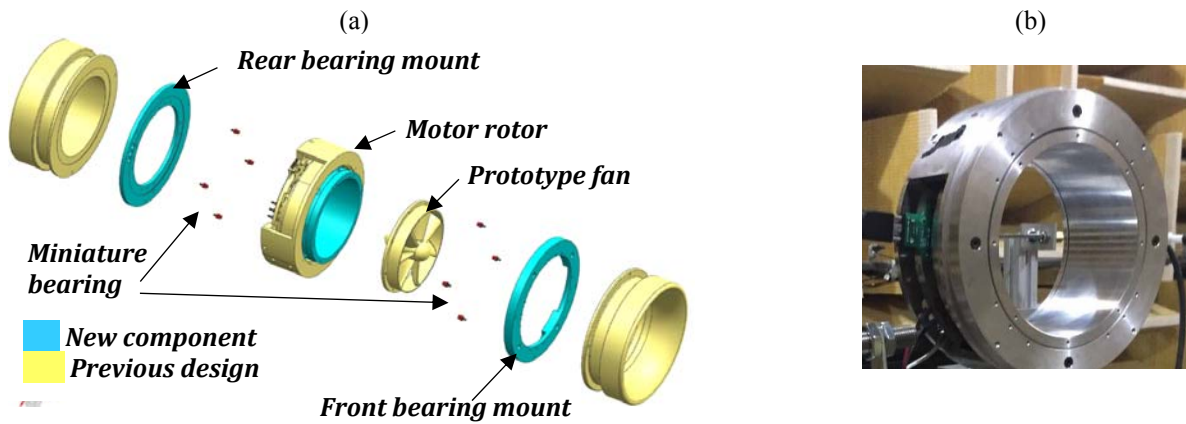
Figure 13: Test Rig 2 (a) CAD exploded view, and (b) assembled fabricated rig.

Table 4: Details on the miniature bearings.

| Bearing Model	Max. Speed, rpm	Outside Diameter	Bearing Design	Picture
SKF, R2-5-2Z	71k	0.3125"	Standard metal balls	
VXB, KIT8926	400k	0.3125"	Solid ceramic balls	

The accurate machining of the bearing mounting positions was critical to maintain contact of the bearings with the motor rotor, i.e. the 4 bearings must be in a perfect circle to avoid metal contact between bearings and motor rotor components. In addition, the outer surface of the motor rotor must form a perfect circle too. The flexibly of this design was low due to constraints on integrating the miniature bearings in the previous design of rig 1. Rig 2 reduced the electrical power consumption but it didn't reduce the mechanical noise. Due to the imperfections of machining, there were small gaps between the bearing surface and rotor. These gaps allow slight movement of the rotor and leads to dynamic imbalance and chinking type noise. However, rig 2 demonstrated the feasibility of using the miniature bearings concept.

Rim mounted fan – Rig 3

Test rig 3 was designed to mainly address the mechanical noise in rig 2. Table 5 lists the problems and solutions that were implemented in rig 3. As shown in Figure 14, in this rig 3 the motor and fan are no longer integrated together but separated 18 inch apart (~ 3 times the fan diameter). The intention was to physically separate the noise from the motor and the rig (the fan and bearings) to allow measuring them independently. The ThinGap motor shaft is coupled with the fan shaft to drive the fan. The misalignment in this drivetrain was handle by a high quality shaft coupling that is able to handle high twisting forces and misalignment in parallel, angular, and axial directions. Through proper assembly, the misalignment of shaft and fan was minimized as well.

**Table 5:** Summary of problems addressed in rig 3.

Test Rig Version	Problem	Solution in Test Rig 3
Rig 1 & Rig 2	Not possible to separate motor and bearing noise contributions.	Shaft drive train design to separate the motor and bearings.
Rig 1	High friction and energy consumption from large bearing	Miniature bearings to support the rotor form outside
Rig 2	Non-firm contact between bearing and the motor rotor	Adjustable bearing mount with 3 bearings
Rig 1 & Rig 2	Imperfections in machining, e.g. off-concentric components, non-perfect circular shape on the rotor O.D.	3 bearings configuration that always are on a perfect circle.
Rig 2	Metal to metal contact noise	Local noise treatment on bearings
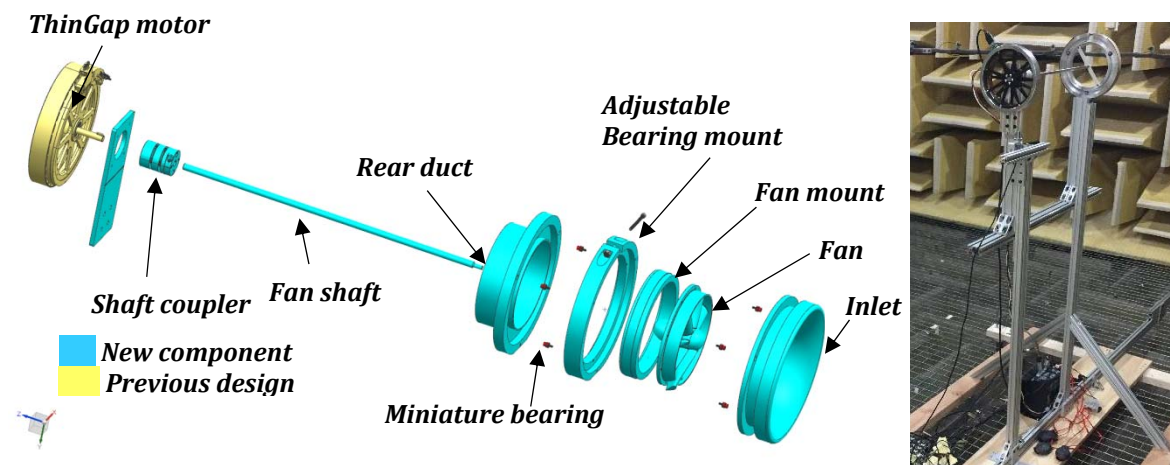
Figure 14: CAD exploded view of test rig 3 and assembled hardware.

As shown in Figure 15, another unique feature of this rig is that the bearing mount ring diameter was designed to be adjustable, i.e. diameter can be changed using the screw at the top of the bearing mount

ring. Furthermore, three bearings are used to hold the fan mount. Since three points always creates a perfect circle, it guarantees continuous contacts between the bearing and the fan mount. This approach allows controlling the contact force between bearings and fan mount. This design offered great flexibility on experimenting different size bearings and vibration/noise treatment of the bearing and the fan mount ring. The best approach to reduce contact noise between the bearings and the fan mount ring was determined to be viscoelastic O-rings mounted on the bearings (Figure 15b). However, this approach introduced problems during high speed operation (>2500 rpm). The main issue was that the O-rings would either fail or separate from the bearing. The O-rings on the miniature bearings in rig 3 achieved 3 dB of noise reduction consistently relative to the original rig 1.
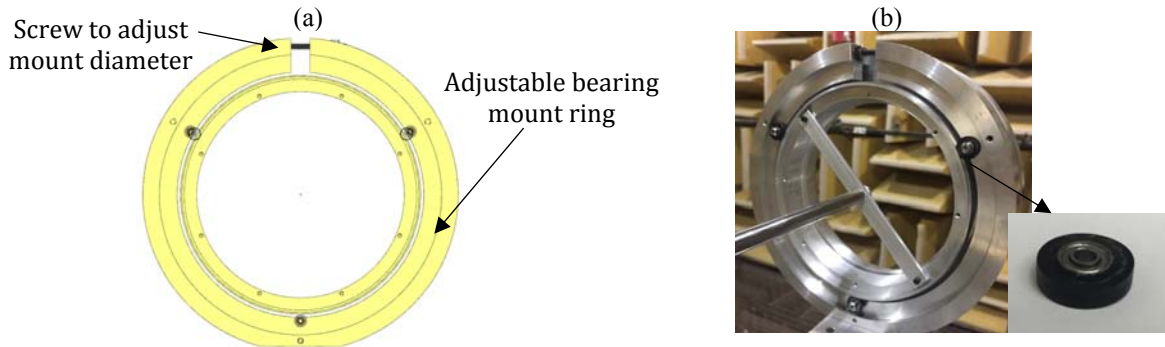
Figure 15: Adjustable bearing mount ring (a) CAD and (b) hardware.

Rim mounted fan – Rig 4

The final small rig 4 was essentially an improved version of rig 3 by implementing a precise adjustment of the motor position, an adjustable distance between motor and fan, and a stiffer support structure (Figure 16). Rig 4 had dual shaft round rail linear guide system on a perfectly flat support plate. In addition, the motor was mounted on an x-y-z-r positioning table that provided highly precise X-Y-Z translational and angular rotation motions. This approach allowed fine adjustment of the motor to achieve better alignment than in rig 3. The distance between motor and fan could also be adjusted. In this rig 4, the fan was operated continuously without any failure at 5000 rpm. This speed was higher than the design speed planned for the realistic quiet fan demonstrator (~4000 rpm). Therefore, rig 4 was the most effective design that also yields minimum rig noise levels.
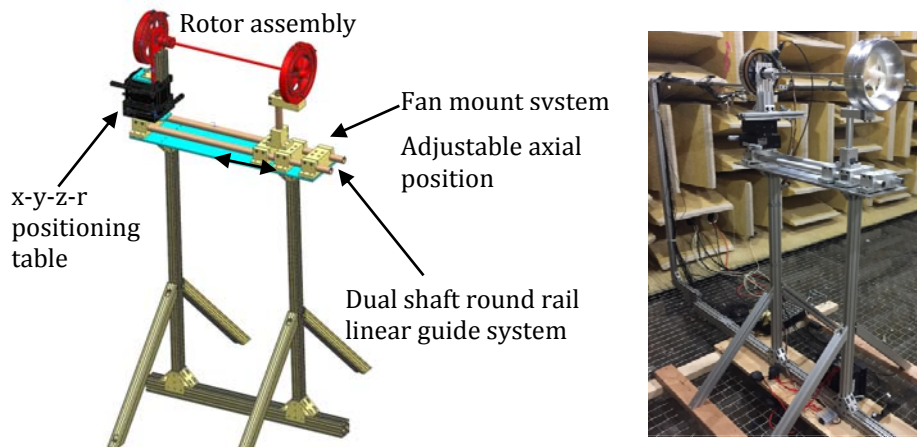
Figure 16: CAD of rig 4 CAD model and hardware.

3.2　Commercial ventilation fans and baseline fan characterization

This section presents the characterization of the commercial ventilation fan that was used as a baseline fan. The purpose of selecting a baseline fan is to establish a reference to define the performance goals to meet in the design of the VTQR fan as indicated in the specific aim: "*a 15-20 dB noise reduction while maintaining/improving aerodynamic performance and electrical power consumption*".

3.2.1　Baseline fan selection

The commercial fan selected as the baseline fan was the Cincinnati model 24631 manufactured by Cincinnati Fan & Ventilator Co. which is shown in Figure 17. The Cincinnati fan has 6 blades and a diameter of 24 inches (0.610 meters). The Cincinnati fan was chosen because its sound intensity level (sound power level normalized by the size of the fan) is representative of the trend in the design of temporarily mounted axial flow ventilation fans. As illustrated in Figure 18, the Cincinnati fan resides exactly on the trend line of the data collected for commercial ventilation fans. Additionally, the Cincinnati fan was chosen because it is manufacturer by one of the leading manufacturers in industrial fans. The fan specifications for the Cincinnati fan are shown in Table 6.

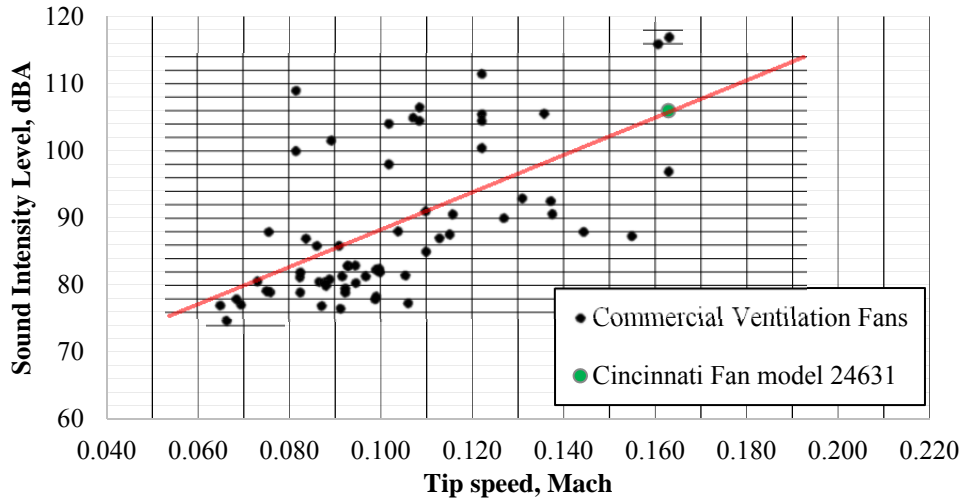**Figure 17:** Cincinnati fan/model 24631.

Figure 18: Sound intensity level vs tip Mach number for commercial fans.

Table 6: Cincinnati fan/model 24631 manufacturer specifications.

| Fan diameter (in)	Motor power (watts)	CFM	SPL @ 10 ft (dBA)	Sound power level (dBA)
24 in.	750	7890	83	100.6

19

An important parameter from the fan datasheet was the sound pressure level of 83 dBA at 10 ft from the source. Assuming spherical waves, the relationship between sound power level and sound pressure level is

$$L_w = L_p(R) + 10\log_{10}(2\pi R^2)$$

where $L_p(R)$ is the sound pressure level at a distance R from the center of the source and $2\pi R^2$ is the surface area of the hemisphere in which sound propagates. Thus, the estimated sound power level of the Cincinnati fan reported by the manufacturer was 100.6 dBA as shown in Table 6.

3.2.2 Test and Results of Baseline Fan

The baseline fan was tested to assess its performance rather than relying on the data reported by the manufacturer as well as to get more in-depth data. To this end, measurements of the radiated noise, flow profile, and electrical power consumption were performed. As shown in Figure 19, the noise tests were performed outdoors due to the large size of the fan. To reduce reflections from nearby objects, a 3.5 feet tall and 8.5 ft wide wall of acoustic wedges was built on two sides of the fan. The measurements were made with an arc array of 19 microphones evenly distributed along its circumference. In order to get an accurate estimate of the sound field generated by the fan, measurements were made at three different angles, 90, 45, and 0 degrees as shown in Figure 20.
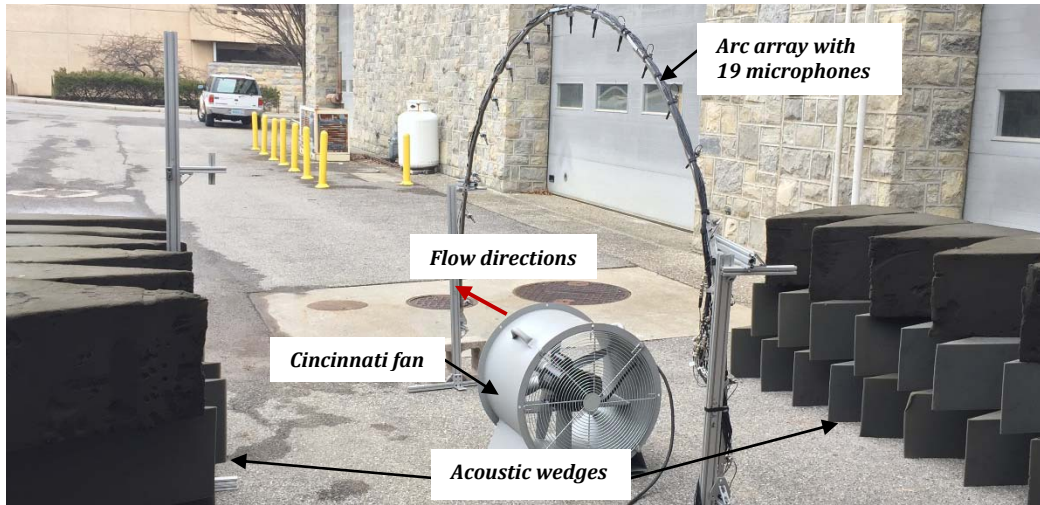

**Figure 19:** Baseline Cincinnati fan experimental set-up.
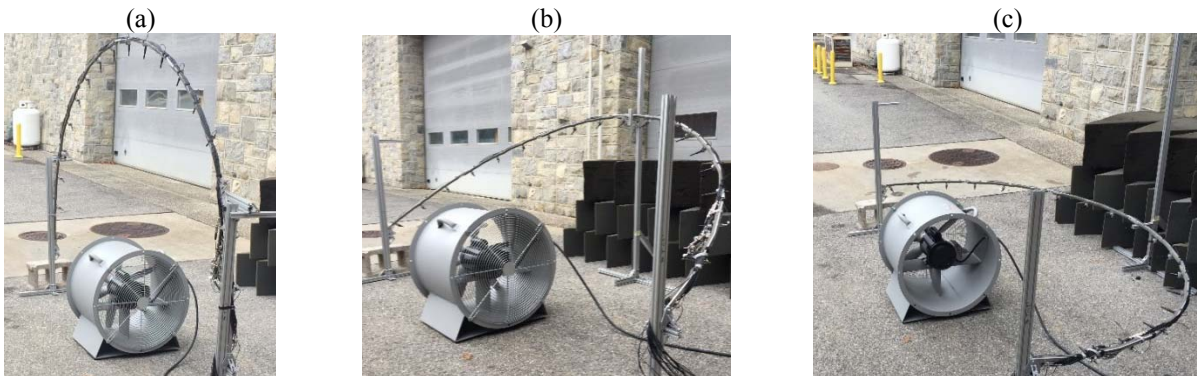
Figure 20: Noise measurements using the microphone arc array at a (a) 90, (b) 45, and (c) 0 degree angle.

The flow and electrical power measurements made are shown Figure 21. An anemometer and traverse system were used for exit flow measurements as shown in Figure 21a. A total of 13 flow measurements were made along the diameter of the fan as shown in Figure 22 (0", ±3.5", ± 4.5", ± 6.0", ±7.5", ± 9.0", and ±11.0"). The power measurements were made with the power analyzer shown in Figure 21b.

(a)   (b)
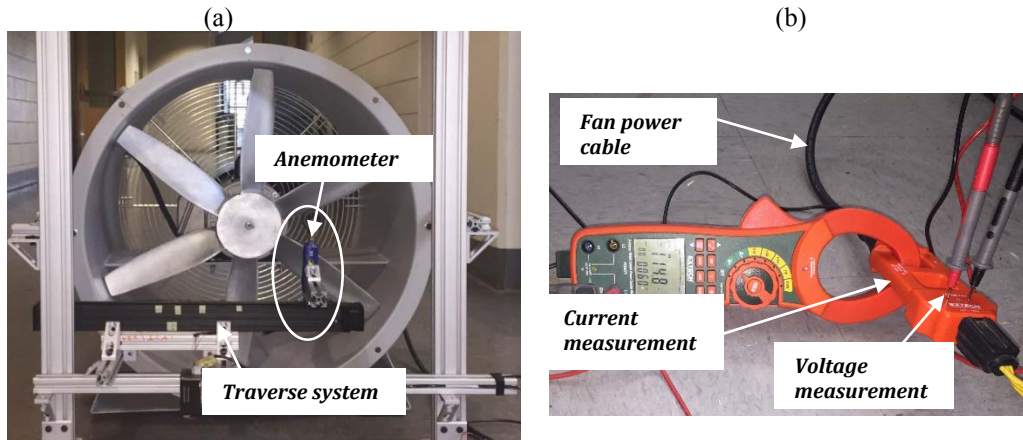
Figure 21: (a) Anemometer and traverse system for flow measurement and (b) power analyzer for fan electric power measurements.
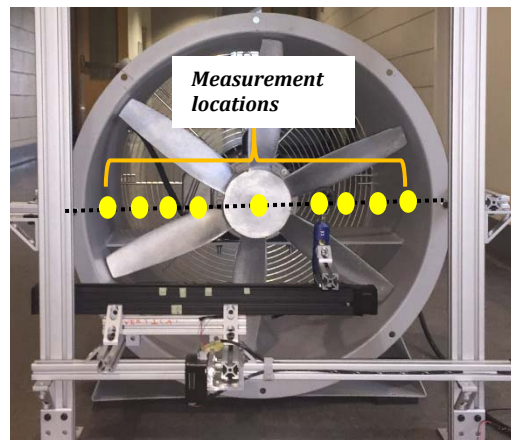

Figure 22: Cincinnati fan flow measurements map.

Since the fan operated at only one speed (1750 rpm), measurements were performed only at this nominal speed. The results from the characterization of the Cincinnati baseline fan are summarized in Table 7. In this table, the measured data was compared to the values reported by the manufacturer in the specification sheet. It was observed that the measured flow rate was about 8% lower, electrical power consumption 17% higher, and sound power level 2.3 dB lower than reported in the specifications.

Table 7: Cincinnati fan characterization main results.

|	Angular velocity [RPM]	Electrical power consumption [watts]	Volumetric flow rate [CFM]	Overall Sound power level [dBA]
Manufacturer Specifications	1750	750	7890	100.6
Actual Measurements	1750	910	7311	98.3

The measured axial flow profile is shown in Figure 23. It shows that the fan generated most of its flow in the center section of the blades. There are significant losses in the center of the duct due to the motor blockage and at the blade tips due to the large tip gaps, thick boundary layer, and potentially poor blade design.
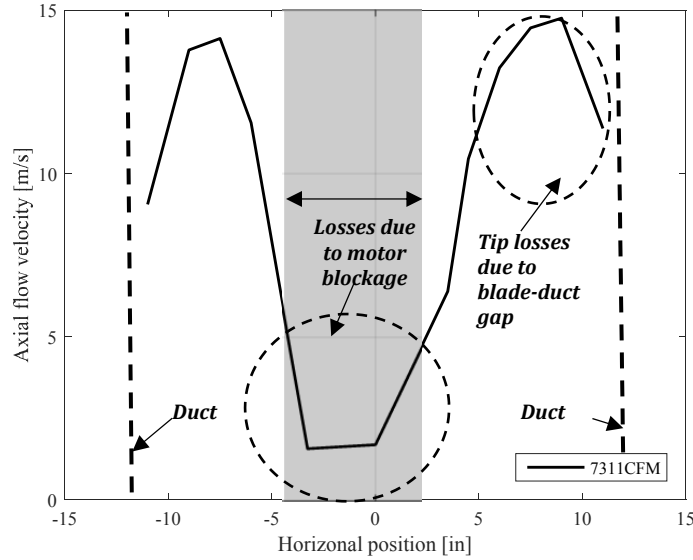
Figure 23: Baseline fan axial flow velocity profile.

The measured sound power level spectrum in 1/3rd octave bands is shown in Figure 24a. To gain better insight, the narrowband spectrum is shown in Figure 24b. All the tones in the spectrum are the fan blade passage frequency (BPF) and the harmonics. Using the noise data recorded, the angular velocity of the Cincinnati fan was also determined from the BPF tone frequency. The BPF was found to be 175 Hz, which corresponds to an angular velocity of 1750 RPM. This agreed very well with the reported speed in the datasheet.
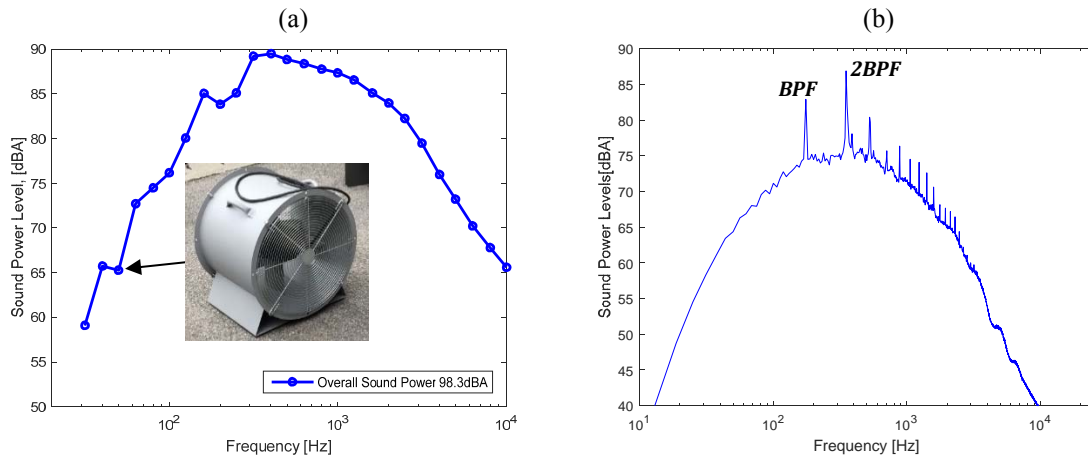
Figure 24: Baseline fan Sound power levels in (a) 1/3rd octave bands and (b) narrowband (6.25 Hz resolution).

3.3 Phase II: Large Scale fan demonstrator

In phase II, the VTQR fan was designed, built, and tested. The VTQR was designed to allow for testing as both rim-mounted and free-tip configurations as shown in Figure 2b.

3.3.1 Fan Design

A new fan design approach was implemented in this Phase II. In Phase I, the classical free vortex design (FVD) method used. In Phase II, the approach was the less conventional controlled vortex design (CVD) technique that resulted in a better design of the blade sections at higher radii. This CVD method allowed the fan to maintain the aerodynamic performance while reducing the fan tip speed. In addition, an optimization code using the E214 airfoil was developed that resulted in the design of a lower tip speed fan with a diameter of 0.362 m (14.25 inches). The design target for the VTQR fan design was to outperform the baseline fan aerodynamically and acoustically. Thus, the VTQR fan was designed to be 15-20 dBA quieter (78.3 to 83.3 dBA) while generating a comparable flow rate (7311 CFM) with the same or less electrical power (≤ 910 watts).

Since the CVD methodology was critical to the design, it is briefly described here. The CVD fan blades are characterized by a span wise changing circulation that ensures a higher flow rate contribution of the blade outer sections, i.e. axial flow increases from the blade hub to the tip. However, a non-uniform span wise circulation is susceptible to radially outward flow that increases near tip losses if the flow is not in radial equilibrium. Consequently, the effect of radial flow was incorporated into the design procedure. To that end, the velocity profile was designed to maintain radial equilibrium and to maximizing the volumetric flow rate.

Due to the varying axial velocity and pressure across the blade for a CVD approach, designing the blades to maintain radial equilibrium is a significant challenge. The challenge is in designing the blade sections so that the centrifugal force of the rotating fluid is balanced by the radial pressure gradient. If there is no radial equilibrium, there will be a radially outward flow that will increases the tip losses and tip stalling (Vad and Horvath, 2008). Therefore, the velocity profile was designed to maintain a radial equilibrium when the following differential equation is satisfied

$$\frac{1}{\rho}\frac{dp_0(r)}{dr} = V_{axial}(r)\frac{dV_{axial}(r)}{dr} + \frac{V_\theta(r)}{r}\frac{d(r*V_\theta(r))}{dr} \tag{1}$$

where ρ is the air density, V_θ is the swirl velocity, V_{axial} is the axial velocity, r is the radial position and $p_0(r)$ is the radial pressure distribution (Dixon and Hall, 2013). To ensure that a non-uniform flow velocity profile maintains radial equilibrium, equation (1) is solved for the axial velocity distribution along the blade, $V_{axial}(r)$, for a prescribed swirl velocity $V_\theta(r)$. The solution to the differential equation in (1) is

$$V_{axial}(r) = \sqrt{2a\Omega(r^{n+1} - r_n^{n+1}) - R(r)*a^2(n+1) + V_{hub}^2} \tag{2}$$

where

$$R(r) = \ln(\frac{r}{r_h})^2 \text{ for } n = 0 \tag{3}$$

23

and

$$R(r) = \frac{r^{2n} - r_h^{2n}}{n} \quad \text{for } n \neq 0 \tag{4}$$

A parametric trade study was undertaken where the axial velocity in equation (2) was investigated to determine the swirl velocity, fan speed (Ω), and the velocity at the hub that will maximize the volumetric flow rate. Figure 25 shows the optimum axial velocity and corresponding swirl velocity as a function of radial position.
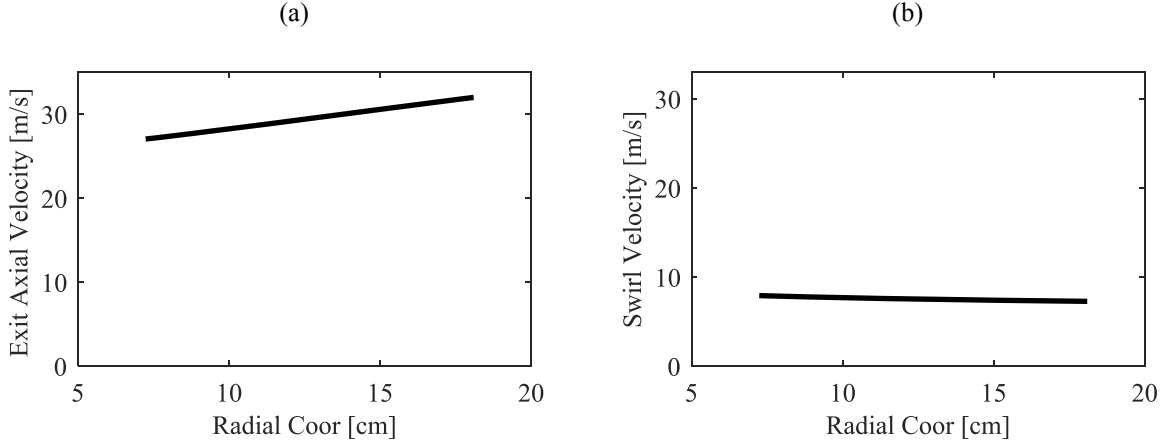
Figure 25: Optimum (a) exit axial velocity and (b) swirl velocity at design speed.

The final design of the VTQR fan required to match as closed as possible the optimum axial and swirl velocities in Figure 25. In addition, geometrical constrains were also implemented due to limitation in the fabrication capabilities at Virginia Tech. They were:

   i.   A maximum fan diameter of 14.25 inches.
  ii.   A blade twist less than 85 degrees at the hub.
 iii.   An axially fan thickness less than 2.5 inches at the tip.

The diameter of the fan was limited to 14.25 inches due to the platform size of the Connex3 3D printer that was used for fabricating the fan. The blade twist was kept below 85 degrees to keep the blade geometry reasonable. Lastly, the fan axial thickness was limited to 2.5 inches due to limitations in the manufacturing capabilities of the outside ring of the fan.

The airfoil chosen for the design of the fan was the E214 airfoil due to its better performance relative to other airfoils considered. Using the hub to tip ratio of 0.4, the blade twist and chord distribution to generate the axial and swirl velocities presented Figure 25 are shown in Figure 26. As illustrated in Figure 26a, the chord distribution is nearly constant with a small increase from the hub to the tip. The blade twist distribution is shown in Figure 26b ranging from 79° at the hub to 42° at the tip. The resulting VTQR fan geometry is shown in Figure 27.
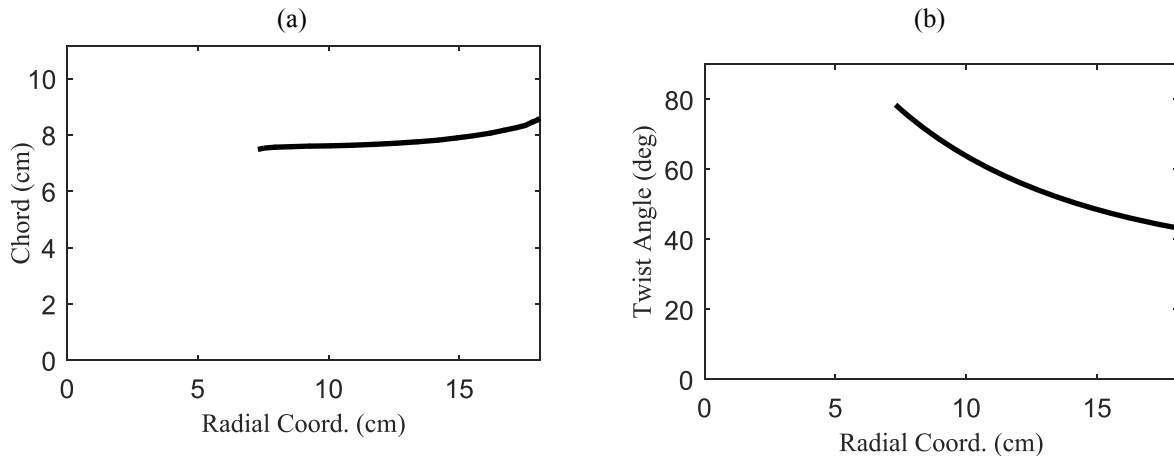
Figure 26: VTQR fan (a) chord, and (b) twist geometry.
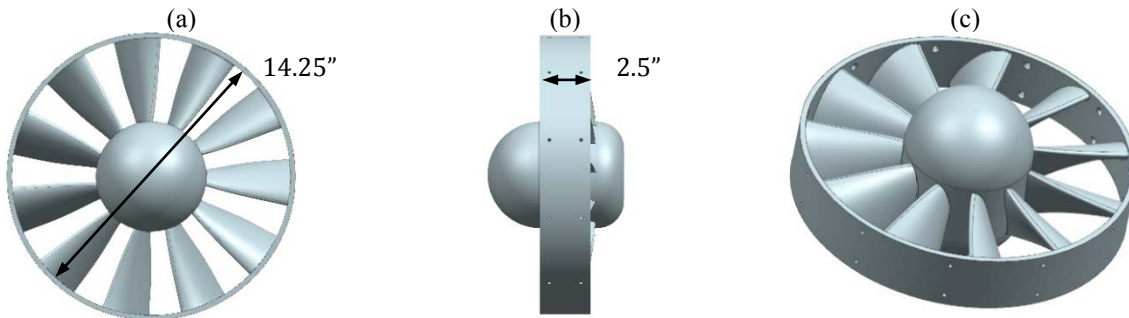
Figure 27: VTQR fan design: (a) front view, (b) side view, and (c) isometric view.

The predicted volumetric flow rate and mechanical power of the fan are shown in Figure 28. As illustrated, the volumetric flow rate and mechanical power at the design speed of 2500 RPM are 5569 CFM and 1820 watts respectively. Additionally, the sound power spectrum for the VTQR fan was computed and shown in Figure 29. As illustrated, the predicted overall sound power level at the design fan speed of 2500 RPM is 70.3 dBA. This indicates a noise reduction of 28 dB relative to the baseline fan. However, this estimate didn't include the noise from the electric motor. Finally, the off design sound power level is presented in Figure 30.
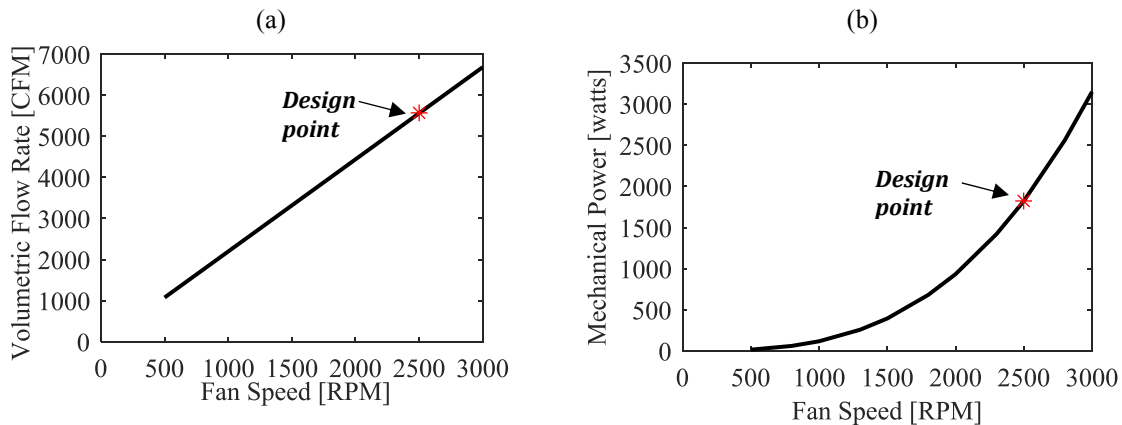
Figure 28: Predicted VTQR fan (a) volumetric flow rate and (b) mechanical power (fan) vs rpm.
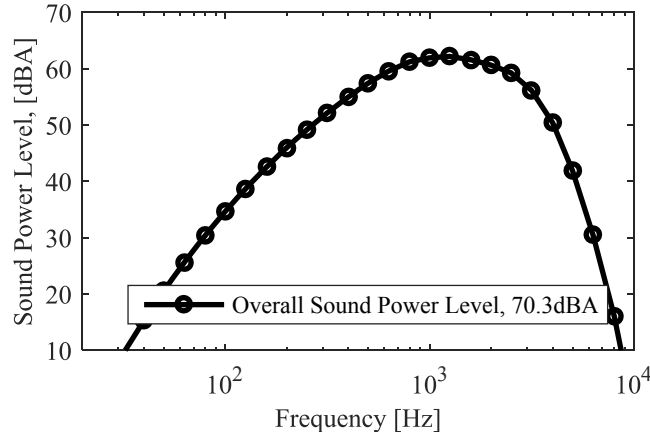
Figure 29: Predicted VTQR fan 1/3rd octave band sound power spectrum.
NOTE: Noise from electric motor is not included..
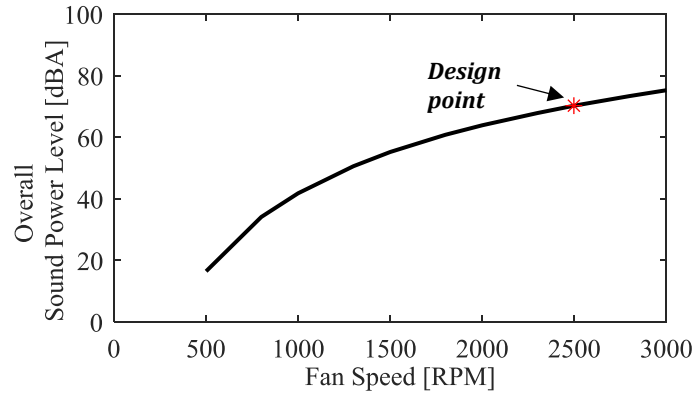
Figure 30: Predicted VTQR fan noise overall sound power level vs rpm.

3.3.2   Design of Duct Geometry

The design the inlet duct geometry of the VTQR fan was also different that for the fans in Phase I. In the small scale fans for Phase I, the inlet duct geometry was a circular bell mouth with the radius as a single design variable. In Phase II, the inlet duct was an elliptical bell mouth with two design variables, the two axes of the ellipse, as shown in Figure 31. As part of the design process, a trade study was conducted to identify the duct geometry that would increase the fan performance and minimizing the duct arc length.

The results of the trade study are shown in Figure 32, e.g. each dot represents an inlet duct design. As illustrated, the volumetric flow rate rise for all of the candidate inlet geometries between 8 and 9%. Thus, it was decided to select the design that has the minimum bell mouth inlet arc length which it was approximately ¼ of the fan diameter. Therefore, the final bell mouth duct geometry had an arc length to diameter ratio of 0.23 and a volumetric flow rate rise of approximately 8%. The final duct geometry incorporated with the fan is shown in Figure 33. The resulting velocity profile with the designed duct geometry was computed and shown in Figure 34 (black line). This velocity profile was adjusted to account for the duct boundary layer. The blue line represents the flow profile without the effect of the inlet duct as computed in section 3.3.1.
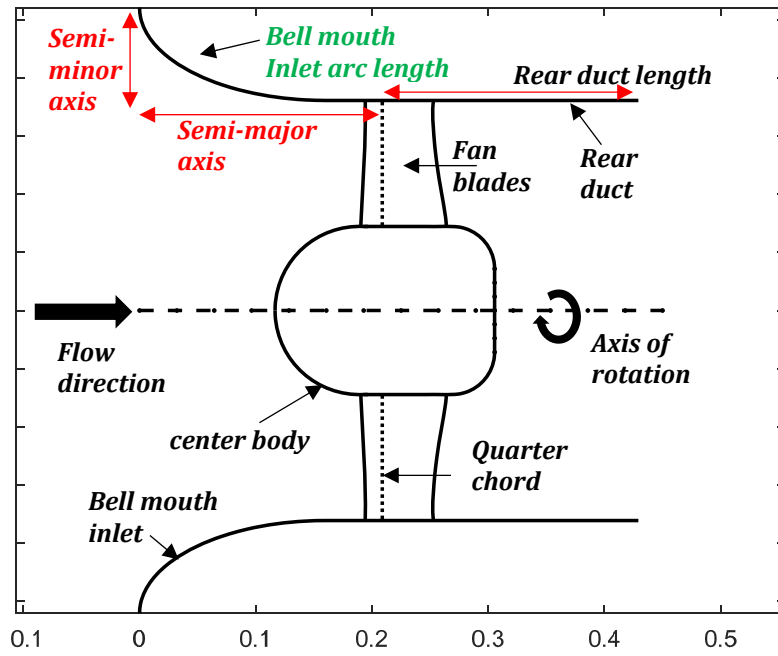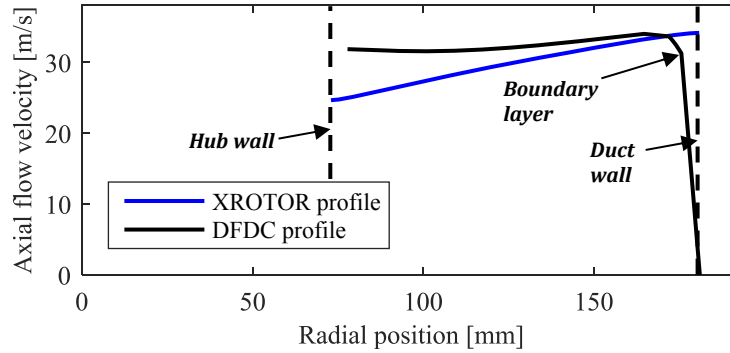
Figure 31: Inlet duct geometry.
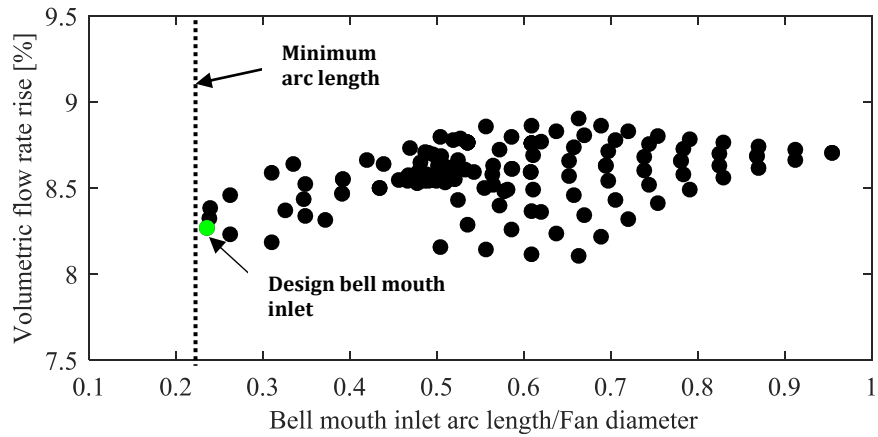
Figure 32: Bell mouth volumetric flow rate improvement [CFM] vs bell length.

Figure 33: Final duct geometry (a) side and (b) isometric view.

Figure 34: XROTOR CVD fan design velocity profile comparison to the DFDC CVD ducted fan velocity profile.

3.3.3   Main differences between Small Scale and VTQR fans

It is important to highlight the main differences between the VTQR fan (Phase II) and the small scale fans (Phase I). They are:

a. The VTQR fan was designed using the controlled vortex design (CVD) method while the small scale fans used the free-vortex design (FVD) method.

b. The VTQR blade twist distribution is significantly lower: from 79º (hub) to 42º (tip) in the VTQR fan compared to 77º to 23º in the Phase I fans.

c. The VTQR blade chord distribution is nearly constant: VTQR hub to tip chord ratio of 0.9 in VTQR fan compared to 1.7 for Phase I fans.

d. The VTQR fan has 11 blades to the 5/7 blades in Phase I fans.

e. The VTQR inlet duct is an optimized elliptical bell mouth. The goal was to maximize flow rate while minimizing the size. The Phase I fans had a simpler circular bell mouth.

3.3.4   VTQR fan demonstrator

The VTQR fan demonstrator incorporated components from rig 4 of the small scale fan from phase I. The fan and duct for the VTQR fan were fabricated using an Objet500 Connex3 and Fortus 450mc 3D printer, respectively. The VTQR fan was 3D printed using the same RGD525 material used for the small scale fans. The duct design was 3D printed using the ABS Plus material. The motor used to drive the VTQR fan was again the ThinGap TG7140 Brushless motor used in the Phase I subscale demonstrator. Since the maximum torque of the motor is 4.52 N-m at a maximum speed of 8141 RPM, a gearbox with a ratio of 3 was used to increase the nominal torque to 13.52 N-m at a maximum speed of 2713RPM. This was sufficient to run the fan at a nominal torque of 6.95 N-m and a nominal fan speed of 2500 RPM.

The VTQR fan was tested in the rim-mounted and free-tip configurations. In the first configuration, the fan is supported at the rim with a set of 3 bearing mechanisms as shown in Figure 35. The bearing mechanisms, shown in Figure 36, support the fan. The bearing house has 2 mini-bearings slightly pressed fitted in the cylinder. Then, 7 O-rings (nominal size 206) are slid into the housing. Washers are used for proper spacing and the shoulder screw acts as the fix shaft for the bearing housing. The O-rings were used to minimize metal to metal noise from the direct contact of the metal bearing and the aluminum ring. An additional mini-bearing is used to prevent the fan from moving forward (axial motion). Unlike in the Phase I tests, this mounting mechanism didn't fail at any time.

In the second free-tip configuration, the shaft is mounted directly to the gearbox (no rim support) as shown in Figure 37. Both configurations were tested and it was found that the free-tip was the quieter and consumed less electrical power. Therefore, *the free-tip configuration was the main one used for testing the fan*.
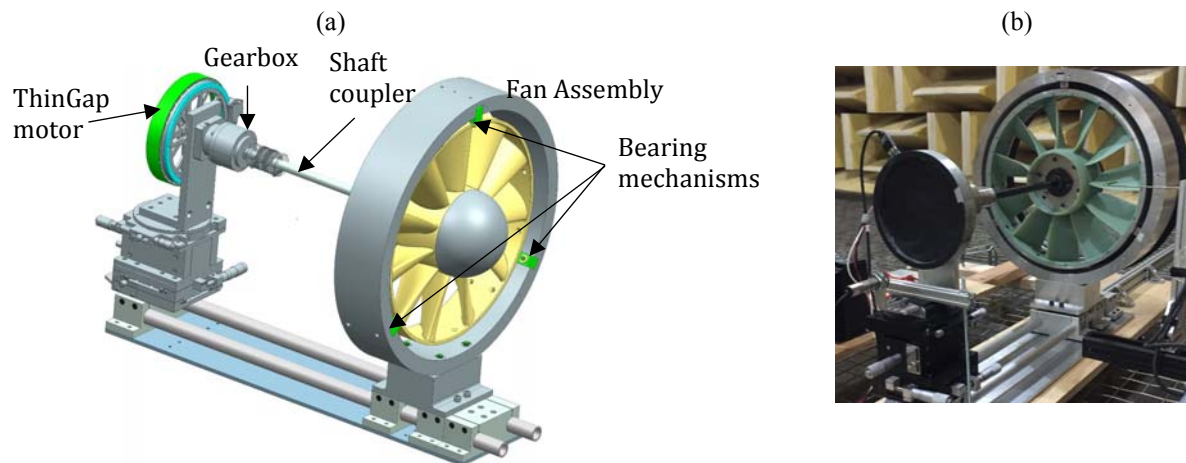
Figure 35: VTQR fan in rim-mounted configuration: (a) CAD drawing and (b) fabricated test rig.
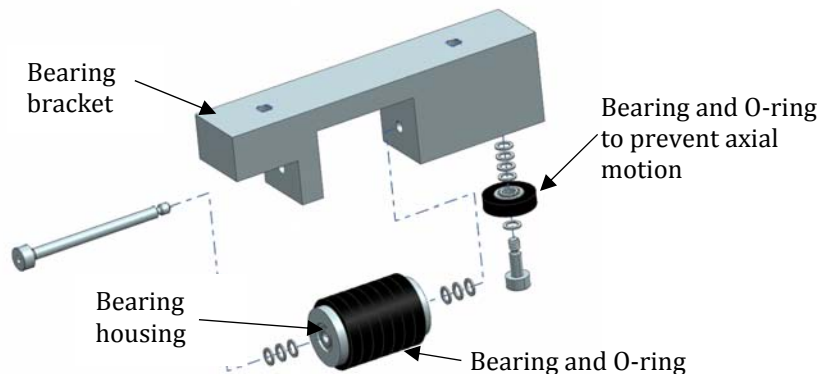
Figure 36: VTQR fan in rim-mounted bearing mechanism.
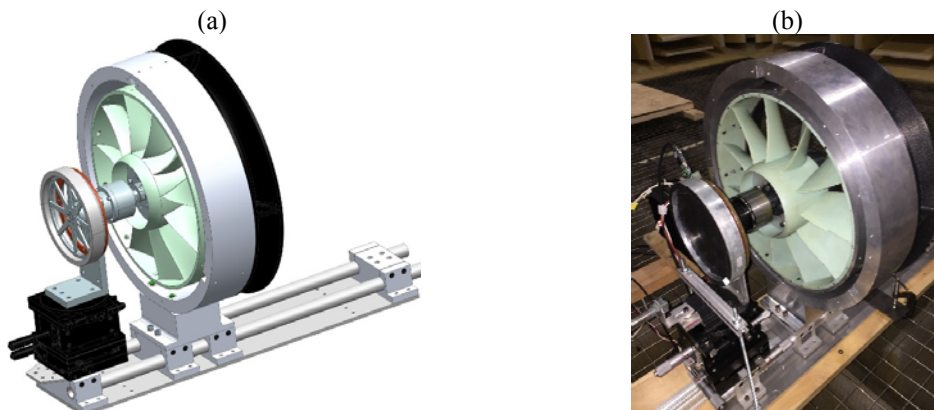
Figure 37: VTQR fan in free-tip configuration: (a) CAD drawing and (b) fabricated test rig.

3.4 Fan experimental set up

Testing of the subscale fan and the VTQR fan was conducted in the anechoic chamber (cutoff frequency of 100 Hz) at Virginia Tech with dimensions of 5.4x4.1x2.4m from wedge tips to wedge tips. The experimental set up for the subscale and VTQR fans are shown in Figure 38 and Figure 39, respectively.

The main noise instrumentation was a 2.8 diameter far-field arc array. The far field arc is composed of 19 microphones evenly distributed along its circumference, i.e. from 0 to 180 degrees. The flow test apparatus consists of a linear actuator, a Pitot-static tube, and a differential pressure transducer. The test set up for the subscale and VTQR fans are shown in Figure 40a and b, respectively. In both phases of the research effort, the Pitot-static tube was mounted on the Haydon LRS linear actuator which it was used to traverse the Pitot-static tube across the duct, e.g. flow velocity profile measurements.

The angular velocity of the fans was recorded using the optical sensor shown in Figure 41. The optical sensor used a laser to measure the time it takes the rotor of the ThinGap motor to complete one revolution. This was accomplished by using a retro-reflective tape that was detected by the optical sensor. The optical sensor signal was connected to a tachometer which displays the fan speed in real time.

The phase current of the ThinGap DC Brushless motor was measured using two different methods. One method was a current monitor function in the B40A40AC PWM servo drive shown in Figure 42a. The current monitor generates an output voltage signal proportional to current output (sensitivity = 5.7 amps per volt). The second method for measuring the current was using a 1-/3-Phase 1000A True RMS AC Power Clamp Meter. The power clamp meter is shown in Figure 42b. The power clamp meter measures the phase current by simply clamping the jaws around one of the phase cables connecting the B40A40AC PWM servo drive to the DC Brushless motor. The current measurements were used to compute the motor torque of the prototype fan using the torque constant provided by ThinGap.

The tests were conducted over a range of speeds, e.g. on and off-design conditions. The testing procedure was to set the fan at a specific speed and perform the direct measurements listed in Table 8. The direct measurements in this table allowed determining the additional system parameters listed in Table 10. The approaches to estimate these additional metrics are also described in the table.
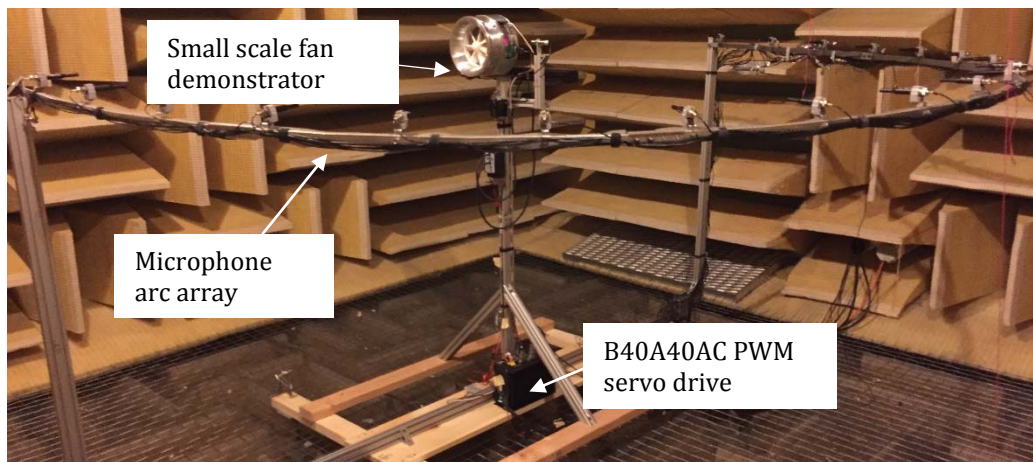
Figure 38: Experimental setup inside anechoic chamber for the small scale demonstrators.
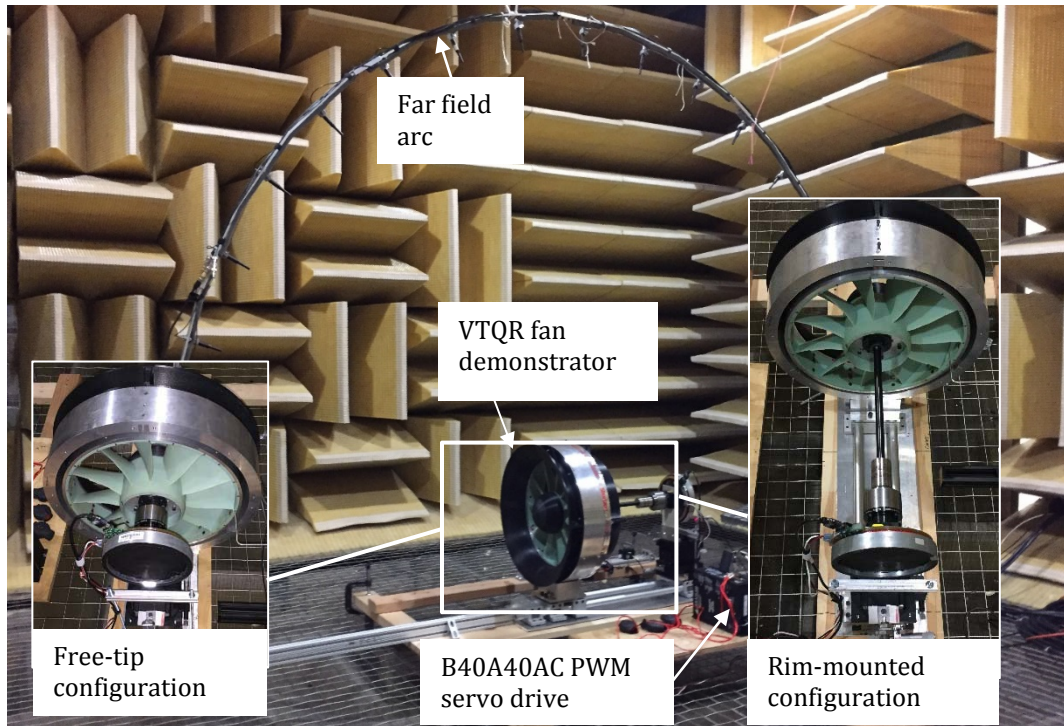
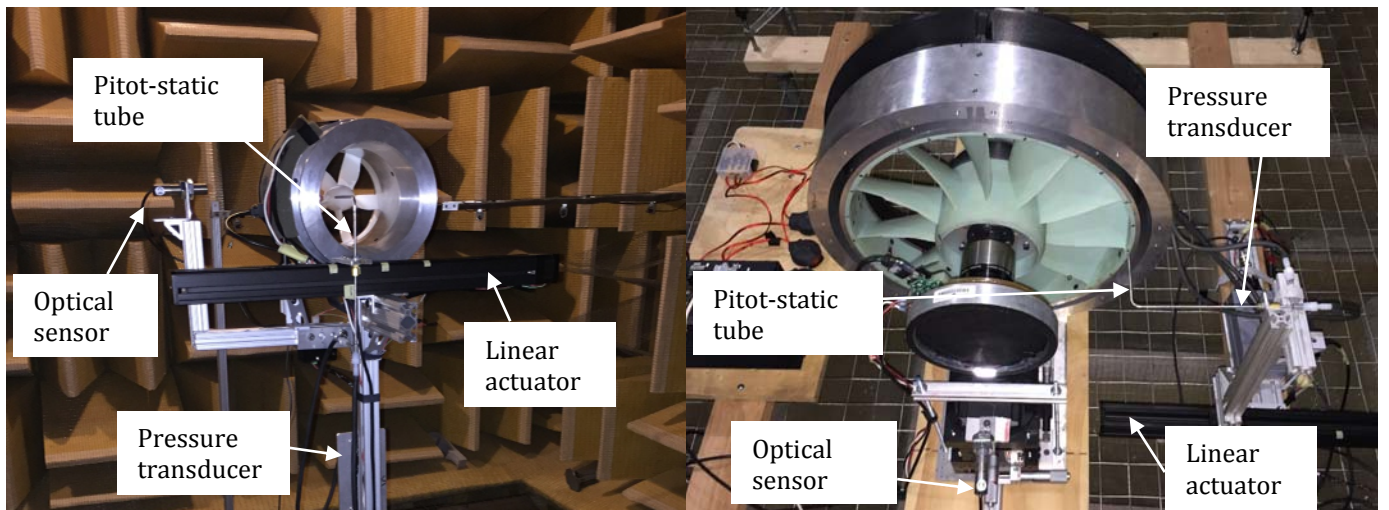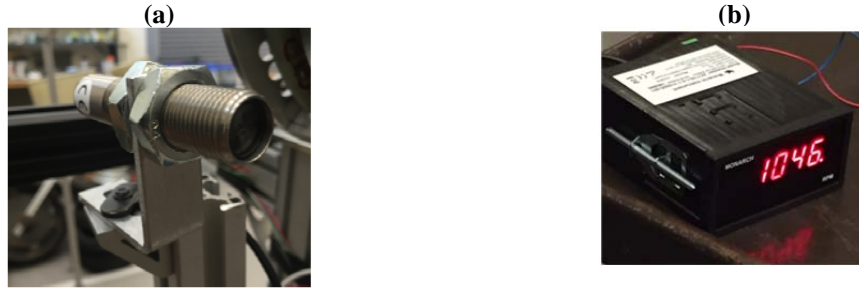**Figure 39:** Experimental setup inside anechoic chamber for the VTQR fan.

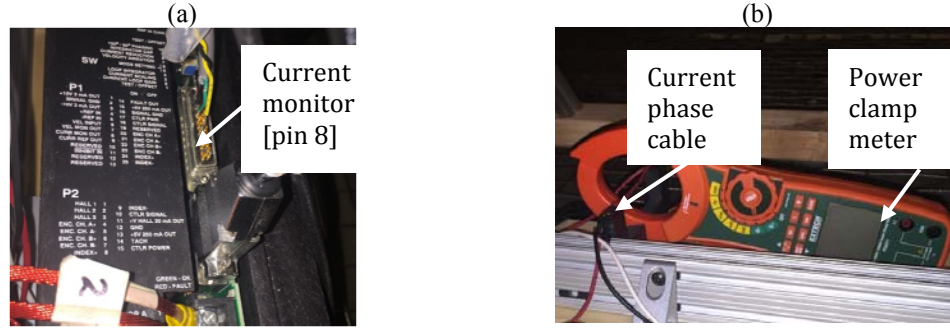(a)   (b)

Figure 40: (a) Small scale fan and (b) VTQR fan demonstrator flow test section.

Figure 41: (a) Optical sensor and (b) tachometer used to monitor fan speed.

Figure 42: Current measuring by (a) measuring current monitor pin of servo drive and (b) power analyizer.

Table 8: List of directly measured parameters.

Parameter	*Measuring instrument(s)*
Speed measurement	Optical sensor with a digital tachometer
Noise measurements	Array of 19 microphones
Exit flow velocity	Pitot-static flow probe and computer controlled traverse system.
Motor phase current	Power analyzer and controller current sensor output channel from the motor controller

Table 9: List of additional parameters obtained from directly measured parameters.

| *Parameter*	*Approach*
Sound and Intensity Power level	The arrays of microphones were used to estimate sound power and intensity levels.
Motor torque	The measured motor phase current and the motor toque constant (k_t provided by ThinGap and independently measured by Virginia Tech) allowed to compute the motor torque as $T_m = k_t \times i_m$.
Motor mechanical power	Product of motor torque and motor speed.
Motor electrical power	Using motor torque, motor RPM, and a validated motor model, the electrical power was estimated.
Fan torque and power	The fan torque and mechanical power of the fans were estimated by subtracting the motor toque (power) of the no-fan configuration to the fan configurations.
Motor efficiency	Ratio of mechanical power to electrical power.

4. Research Findings and Accomplishments:

In this section, the key findings and accomplishments of the project are presented. Following the structure of the project and this report, the findings and accomplishments are also separated into Phase I and II. Main results are also presented to substantiate the findings and achievements.

4.1 Phase I Subscale Demonstrator

4.1.1 Determined the feasibility of rim-driven and rim-mounted fans

One of the key hypotheses of the project was that a rim-driven fan would allow eliminating many noise sources and yielding a very quiet fan. The rim-driven demonstrators (subscale rigs 1 and 2) were found not to be practical with the current technology due to high mechanical noise and excessive amount of electrical power required. The mechanical noise was from the bearings, vibration transmitted to the rig from the motor, and the motor itself. The excessive electrical power was due to significant friction in the large diameter bearings that resulted in the bearings consuming as much as energy as the fan. Consequently, the rim-mounted demonstrators (rigs 3 and 4) were designed to address these problems but primarily the mechanical noise. To this end, modifications were implemented to reduce the noise sources that resulted in the last subscale rig 4. The key changes implemented were the use of 3 miniature bearings with a viscoelastic O-ring mounted to reduce the transmission of vibration to the rig. In addition, an adjustable ring mount was implemented to hold the fan with variable tolerance. Finally, the motor and fan were physically separated and an x-y-z-r positioning table used to provide precise alignment of the motor-fan system. For completeness, Figure 43 shows rigs 1 and 4 with the key changes indicated in the figure.
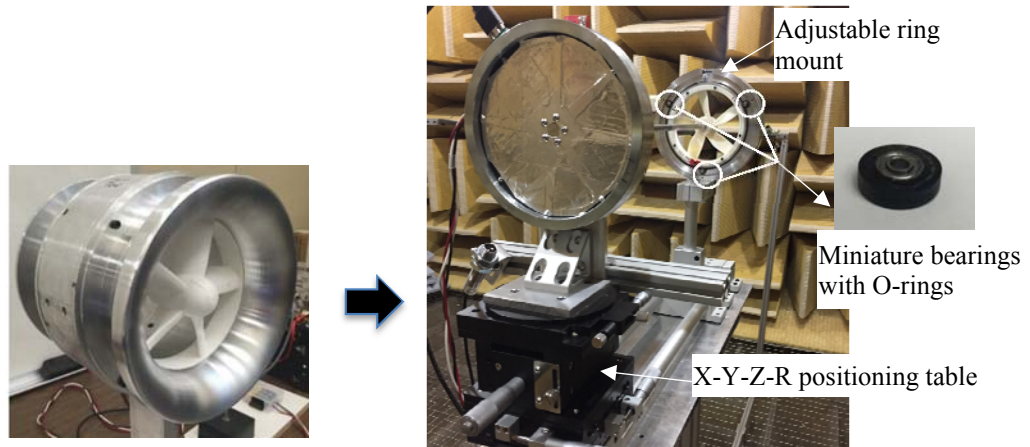
Figure 43: Key changes from rim-driven to rim-mounted fan configuration (from rig 1 to rig 4).

In addition to the rig changes described, noise reduction of the motor and the test rig were also undertaken. The efforts for reducing motor and rig noise are described in depth in Appendix D. The main results of these efforts are illustrated in Figure 44. This figure shows the noise spectrum without and with the noise treatments of the motor/rig system (no fan installed). The results illustrate significant noise reduction of the system demonstrating that there are opportunities to reduce the overall system noise by not only focusing on the fan but the whole system. Note that the first tone at around 70 Hz is produced by the motor and it clearly needs to be reduced. The actual noise mechanisms for this tone is not clear.
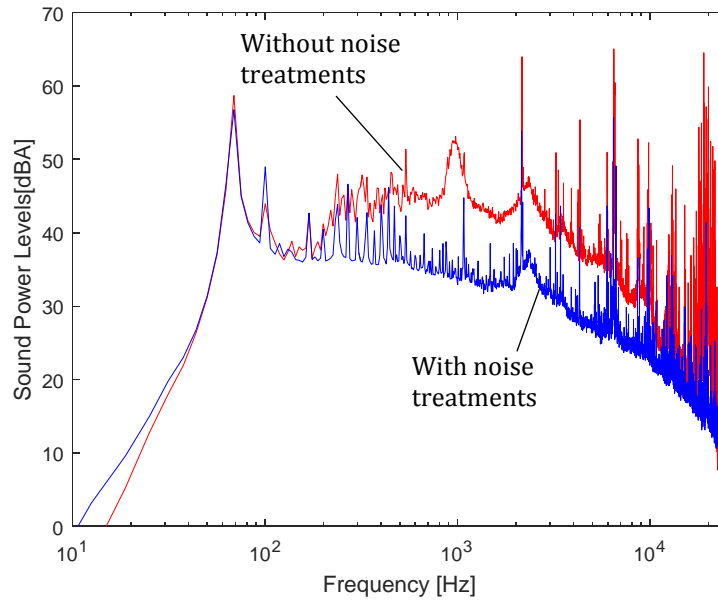
Figure 44: Noise spectrum of the ThinGap motor and rig without (red) and with (blue) noise treatments.

The effectiveness of the efforts undertaken to reduce the noise from rig 1 (rim-driven) to the final rig 4 (rim-mounted) is summarized in Figure 45. This figure shows the measured overall A-weighted sound power level for both rigs as a function of the fan rpm. The key observation is that we were able to reduce the noise of the small scale fan by 10.4 dB at 5000 rpm, from 85.6 dBA for the original rig 1 to 75.2 dBA for the last rig 4. The attenuation was even better at 3000 and 4000 RPM with reductions of 11.5 and 11.7 dB, respectively. Unfortunately, the noise levels for rig 4 were still relative high to achieve the objective of 15 to 20 dB reduction compared to current ventilation fans.

The 1/3rd octave band spectrums for rigs 1 and 4 at 5000 RPM are shown in Figure 46. It can be observed that the reduction is significant (>10 dB) in all 1/3rd octave bands except for certain bands, e.g. 80, 1000, 1250, 2000, 2500, and 3150 Hz. The noise in these bands is due to the motor. For completeness, the spectral results for 2000, 3000, and 4000 RPMs are also shown in Figure 46.
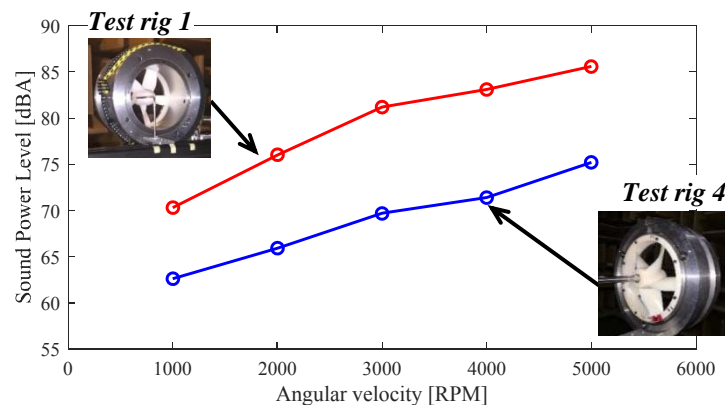
Figure 45: Overall A-weighted sound power level (dBA) as a function of rpm for rig 4 and rig 1 (fan 171).

34
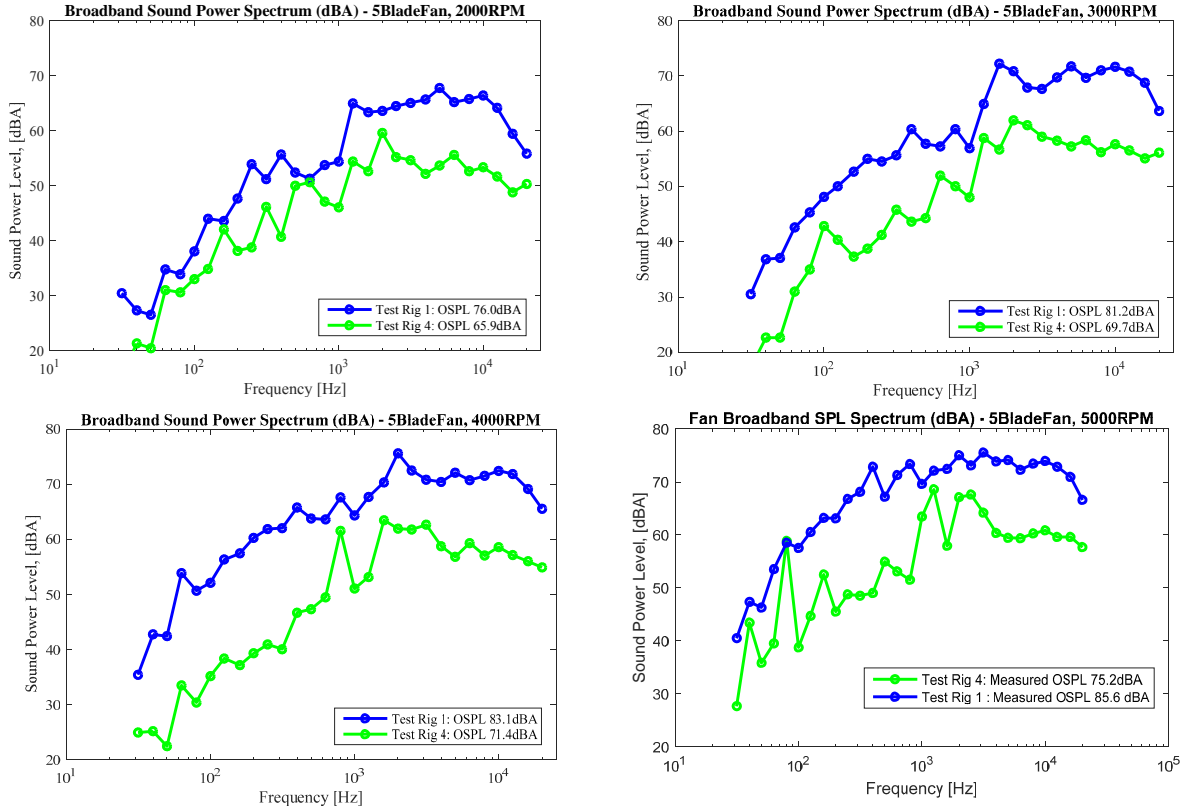
**Figure 46:** Measured sound power levels in 1/3rd octave bands at 2000, 3000, 4000, and 5000 RPM for rigs 1 and 4 (fan 171).

In summary, the work performed in Phase I using rigs 1 through 4 indicated that the rim-driven fan concept cannot be successfully implemented with current technologies to achieve the project objectives. Additionally, key issues with the rim mounted approach were identified. The two main issues identified at the end of the Phase I effort were the noise levels (mainly mechanical) and the durability of the viscoelastic O-rings used in conjunction with miniature high speed bearings. Based on this key finding, the VTQR fan developed in Phase II was designed to be implemented as both rim-mounted and free-tip configurations.

4.1.2 Excellent Aerodynamic Performance of Subscale Demonstrators

The results from the subscale fans (both 171 and 349) demonstrated that they had excellent aerodynamic performance. The aerodynamic performance was determined by measuring the velocity profile along the radius of the duct as illustrated in Figure 47. From the velocity profile, the average axial flow velocity was computed and compared to the data for the commercial ventilation fans. Figure 48 presents the average exit flow velocity as a function of tip fan Mach number for the commercial fans and the subscale fans 171 and 349. For easy of comparison, the commercial fan trend is shown as a red dashed line. As shown in the figure, the subscale fans clearly outperformed all of the commercial fans, i.e. produced a high exit flow velocity. *The significance of this finding is that it implies that a smaller well designed fan can generate the same or more CFM as of larger commercial fans.*

(a)　　　　　　　　　　(b)　　　　　　　　　　(c)
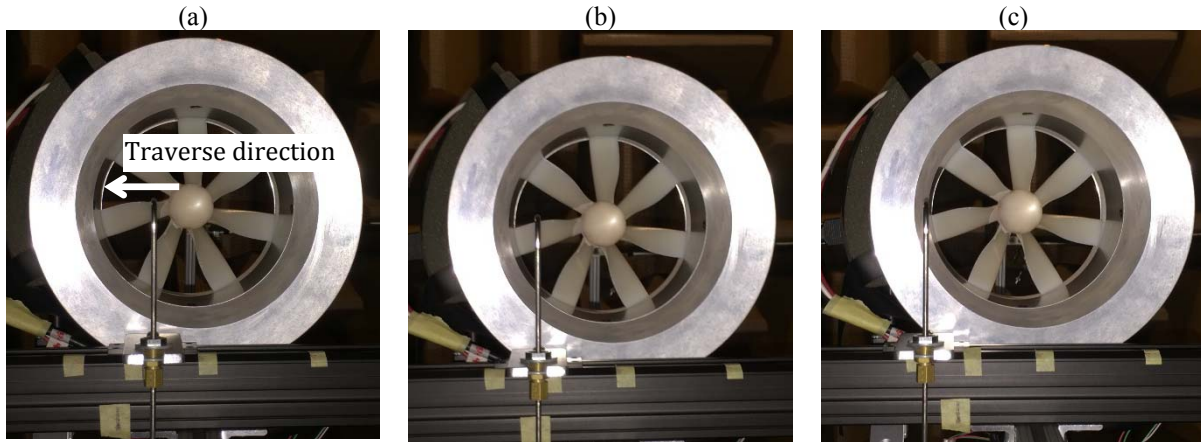
Figure 47: Traverse flow measurements of subscale rig.
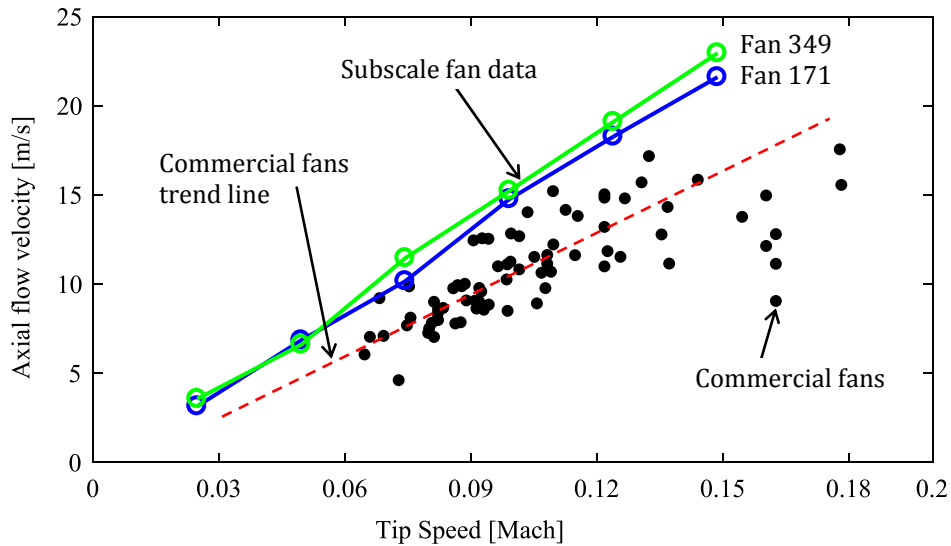
Figure 48: Exit velocity vs fan tip Mach number for commercial (black dots) and the 2 subscale fans (171 and 349).

4.1.3 Validated Aerodynamic Design of Fans

A key reason for the excellent aerodynamic performance of the fans discussed in section 4.1.2 was the proper design of the fans including the effect of the inlet duct. ***Thus, another key achievement of the Phase I was the development of fan design procedures and the selection of accurate aerodynamic prediction tools***. As described in section 3.3.1, two blade design approaches were investigated in this project: the free and controlled vortex design (FVD and CVD) methods. These design approaches and tools were experimentally validated. To illustrate this accomplishment, results for subscale fan 349 are presented in Figure 49 through Figure 51 and compared to predictions. This fan was designed using the FVD method.

The measured and predicted axial flow radial velocity distribution at 6000 rpm is shown in Figure 49. The measured data shows that the flow is nearly uniform, as intended, except on the outer part of the blade towards the duct wall, e.g. the flow gradually slows down as it gets closer to the tip of the fan. The decrease in axial flow at the tip is due to the presence of the turbulent boundary layer. The boundary layer thickness was predicted to be around 13.5 mm and it matches well the measured data. The average

36

axial flow from the measurements was computed and compared to the XROTOR and DFDC predictions. The measured average axial flow across the fan is in very good agreement with the results from DFDC (20 vs 21.5 m/s or 6% error) that accounts for the effect of the inlet duct. On the other hand, XROTOR under-predicts the measured average flow velocity by about 11% (19 to 21.5 m/s).

Since the velocity profile is relatively uniform, additional flow measurements were carried out at a fixed radial position of 46 mm from the center as a function of fan speed. The results are shown in Figure 50. The agreement between the experimental data and the XROTOR predictions is good up to 2000 RPM. Above 2000 RPM, the axial flow measured is higher than the XROTOR predictions. On the other hand, the predictions with DFDC show better agreement with the experimental data at all RPMs. Thus, it is clear that the effect of the duct is more significant at the higher fan speeds. The repeatability of the data was also demonstrated by testing the fan twice several days apart. As shown in the figure, the repeatability is excellent (tests 46 and 50). The final validation of the aerodynamic tools is by comparing the measured and XROTOR predicted fan mechanical power. These results are presented in Figure 51 and they show excellent agreement.
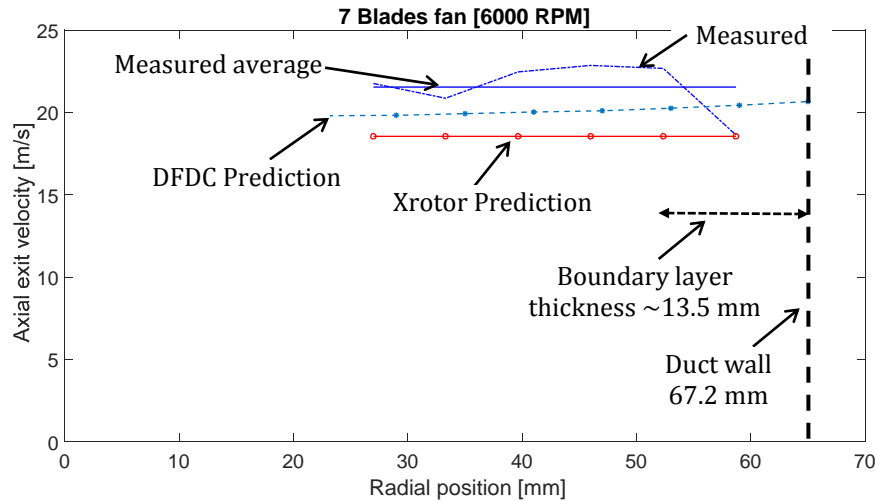
Figure 49: Axial flow velocity profile for fan 349 at 6000 RPM.
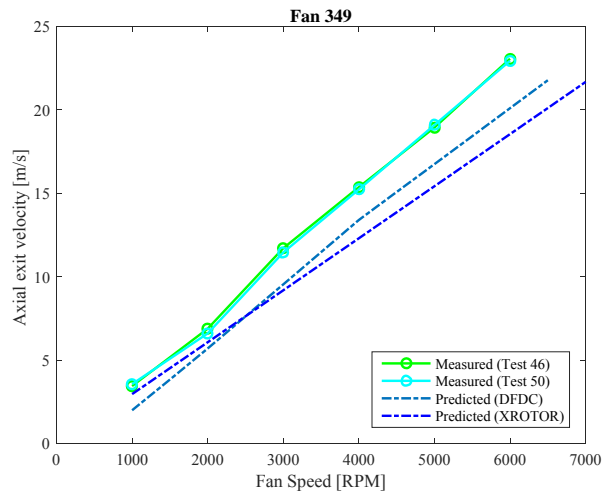
Figure 50: Axial flow velocity at a fixed radial position (46 mm) as a function of fan speed (fan 349).
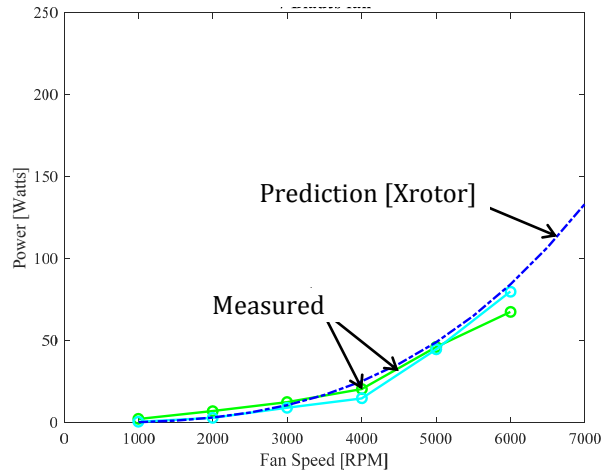
Figure 51: Fan mechanical power vs fan rpm.

4.2 **Phase II VTQR Fan Demonstrator**

4.2.1 *Successful Demonstration of the VTQR fan*
A key premise of this research was that a low tip speed fan with an optimum blade design is the best approach to reduce noise. The VTQR fan demonstrated this premise and thus this is the main accomplishment of the project. To substantiate this claim, the results from the testing of the VTQR fan and its comparison to the baseline fan (Cincinnati) and the other commercial fans are presented next. As a reminder, the VTQR fan was tested in both the rim-mounted and free-tip configurations shown in Figure 2b.

Figure 52 shows a side to side comparison between the VTQR and baseline fans. In this figure, the pictures are properly scaled to visually illustrate the size difference between these two fans. The VTQR fan has a diameter of 0.362 m (14.25 inches) compared to the baseline fan with a diameter of 0.81 m (24 inches). In addition, Table 10 presents a comparison of main parameters of the fans. It is important to remark that the VTQR fan at the design speed (2500 RPM) resulted in a predicted similar volumetric flow rate as the baseline Cincinnati fan at a lower tip speed.

Figure 52: Pictures of the (a) VTQR fan and (b) Cincinnati baseline fan (model 24631).

38

Table 10: Overall comparison of the design performance of the VTQR and baseline (Cincinnati fan/model 24631) fans.

Parameter	VTQR fan	Baseline fan Cincinnati fan/model 24631
Fan diameter	0.362 m (14.25")	0.61 m (24")
Effective cross sectional area	0.0865 m^2	0.244 m^2
Number of blades	11	6
Maximum blade chord	0.085 m (3.34")	0.073 m (2.87")
Blade tip/hub ratio	0.4	0.2
Blade tip twist angle	43 deg	30 deg
Blade camber	4.03%	0%
Tip gap	0 m (0")	6.35 mm (0.25")
Inlet duct diameter	0.4788 m	No inlet duct
Fan speed at design	2500 RPM	1750 RPM
Fan tip Speed at design (Mach)	0.14	0.165
Fan volumetric flow rate at design speed	6020 CFM	7311 CFM

Due to motor power limitations, the VTQR was tested at a maximum speed of 1766 RPM rather than the design speed of 2500 RPM. The reason was due to an unforeseen under performance of the ThinGap motor due to poor current-voltage matching from the manufacturer. We were expecting the ThinGap motor to operate the fan to a maximum speed of 2700 RPM.

The measured performance comparisons between the VTQR fan demonstrator in the free-tip configuration and the baseline fan is summarized in Table 11. The VTQR results in this table were for a speed of 1616 RPM since it resulted in exactly half the CFM of the Cincinnati fan. Table 11 compares the key performance metrics established in the project objectives, namely overall noise levels (dBA), volumetric flow rate (CFM) and electrical power consumption (watts). The proposed targets for these metrics to assess the success of the project are also listed in the table in the 5th row. They were a reduction in the overall A-weighted sound power level of 15-20 dBA relative to the baseline fan with the same (or more) flow rate and (or less) power consumption.

Due to the power limitation, the VTQR fan at 1616 RPM achieved a volumetric flow rate of 3665 CFM (rather than the 6020 CFM expected at 2500 RPM). Consequently, an array of two VTQR fans is required to match the volumetric flow rate of the baseline fan (7311 CFM). Therefore, the results in Table 11 include the case of a single and two VTQR fans. As expected, two VTQR fans will increase the noise levels from 77.8dBA for one fan to 80.8 dBA ($77.8 + 10\log(2)$) for two fans as shown in Table 11. Therefore, the two VTQR fans at a fan speed of 1616 RPM would generate the same volumetric flow rate as the baseline fan while reducing noise levels by 17.5 dB. However, the two VTQR fans do consume more electrical power, 1510 watts vs the 910 watts for the Cincinnati fan. This is a rather unexpected result which we attributed to the poor performance of the ThinGap motor, e.g. low efficiency. The other possibility is from losses in the gear reduction which it is very unlikely since efficiency of the gear is reported at 97%.

Table 11: VTQR and baseline (Cincinnati fan/model 24631) fans performance comparison.

Fan	Angular velocity in RPM (Tip Mach)	Overall Sound power level [dBA]	Volumetric flow rate [CFM]	Electrical Power [Watts]
1 VTQR fan (measured)	1616 (0.09)	77.8	3665	755
2 VTQR fan (measured)	1616 (0.09)	80.8	7330	1510
Baseline fan (measured)	1750 (0.162)	98.3	7311	910
Project Targets	NA	15-20 dBA lower	Same or more	Same or less
Improvement (using 2 VTQR)	NA	17.5 dBA lower noise	Same (0.25% more)	40% more

To gain better insight into the VTQR fan noise performance, Figure 53 shows the measured 1/3rd octave band sound power spectrum for both the VTQR and the Cincinnati fans. The results for both 1 and 2 VTQR fans are shown in the figure. It is clear that the VTRQ fan is significantly quieter than the Cincinnati fan for all 1/3rd octave bands below 5000 Hz. For example, at 1000 Hz the attenuation is ~ 18 dB. The noise levels above the 6300 Hz band are virtually the same for both fans. It is also important to note that the noise from the ThinGap motor (which it was not acoustically treated) dominates the VTQR fan spectrum at the 80 Hz band and the 1000 Hz and higher bands. The peak at the 315 Hz band is due to tonal noise from the fan.

Figure 54 shows a comparison of the axial flow velocity radial distribution for the two fans (VTQR and Cincinnati). Since the two fans have different diameters, the axial velocity is plotted as a function of the radial position normalized by the duct diameter. The figure shows that the VTQR fan is generating significant larger flow velocities than the Cincinnati fan, e.g. maximum axial flow of 24 m/s vs 15 m/s. Thus, the plots in this figure explains why with a smaller fan generates similar flow rate as the larger Cincinnati fan. This implies that the VTQR fan is more aerodynamically efficient than the Cincinnati fan.
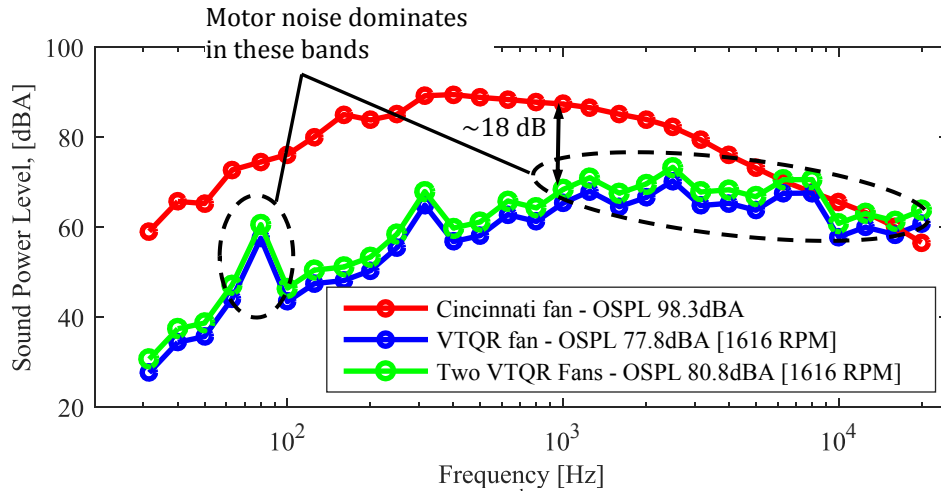

Figure 53: VTQR and Cincinnati fan measured 1/3rd octave band sound power spectrum comparison.
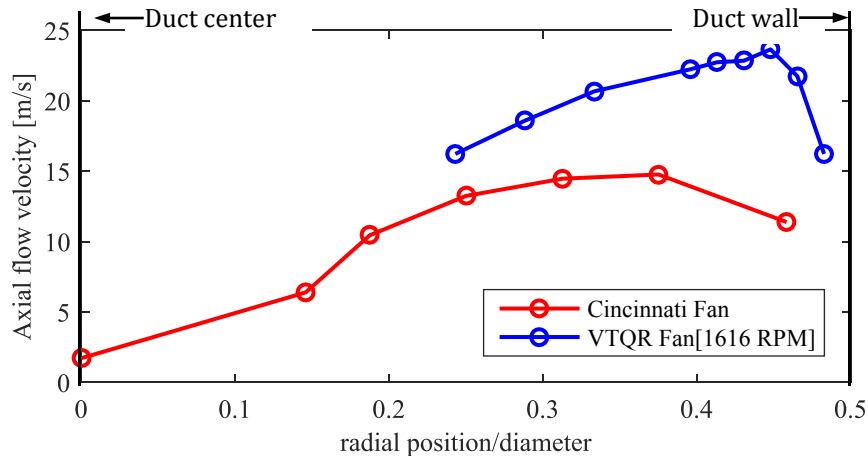
Figure 54: VTQR and Cincinnati fan measured axial velocity profile comparison vs normalized radial position.

Additionally, the axial flow of the VTQR fan is compared to data commercial ventilation fans. Again Figure 55 shows the average axial flow velocity as a function of the fan tip Mach number. It shows that the VTQR fan demonstrator outperforms aerodynamically all commercial ventilation fans by a significant margin. As a reference, the result for the subscale fan 349 is also shown in the figure. The VTQR fan also has a better aerodynamic performance compared to the subscale fan demonstrating that the CVD method is better than the FVD approach used in the subscale fans.
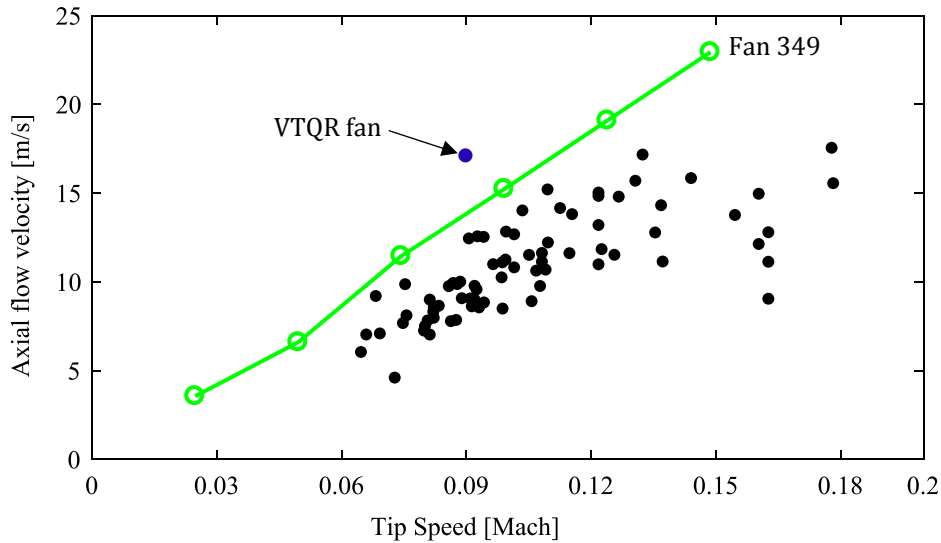
Figure 55: Exit velocity vs fan tip Mach number for commercial (black dots),
VTQR fan (blue dot), and the subscale fan 349.

The VTQR and Cincinnati fan volumetric flow rate and noise comparisons in Table 11, Figure 53, and Figure 54 provide only a partial picture of the VTQR performance. To this end, the VTQR fan is also compared to all the commercial fans. In Figure 56, the sound power level is plotted as a function of the volumetric flow rate for a large number of commercial ventilation fans. The sound power level and

41

CFM for these commercial (CFM) fans were obtained from published manufactured data, e.g. data was assumed accurate. The results for the VTQR fan is also included and labeled (green dot). As shown in the figure, the VTQR fan at the measured fan speed (1616 RPM) outperforms most of the commercial fans in terms of noise and/or CFM. The few commercial fans that are quieter and generate more CFM than the VTQR fan are inside the shaded area in the plot. The fan diameter for these fans is also indicated in the figure. It is noticeable that all of these fans have dimeters that are between 25% and 100% larger than the VTQR fan, i.e. 0.45 to 0.71 m versus 0.362 m for the VTQR fan. Additionally, it is important to note here that at the fan design speed, the VTQR fan is predicted to generate a volumetric flow rate of 6020 CFM with a fan sound power level of 70 dBA as shown in Figure 56 (yellow dot). However, it is important to note that the noise level includes only the fan noise, e.g. mechanical noise and motor noise not included in this estimate. Although not experimentally verified due to motor power limitations, it helps to establish a potential lower bound for the noise (if motor noise is reduced) and illustrate the capability of the VTQR fan.

In summary, the VTQR fan was designed to lower the fan tip speed while maintaining the aerodynamic performance and restricting the size of the fan diameter. The compactness of the design is a desirable attribute since floor space restrictions in working areas can significantly restrict the fan size to use (Lawrence Berkeley National Laboratory, 1989). ***Consequently, the compact VTQR fan can significantly contribute to the improvement of the health and safety of mine workers by providing a high volumetric flow rate at low noise levels in a constrained work environment.***
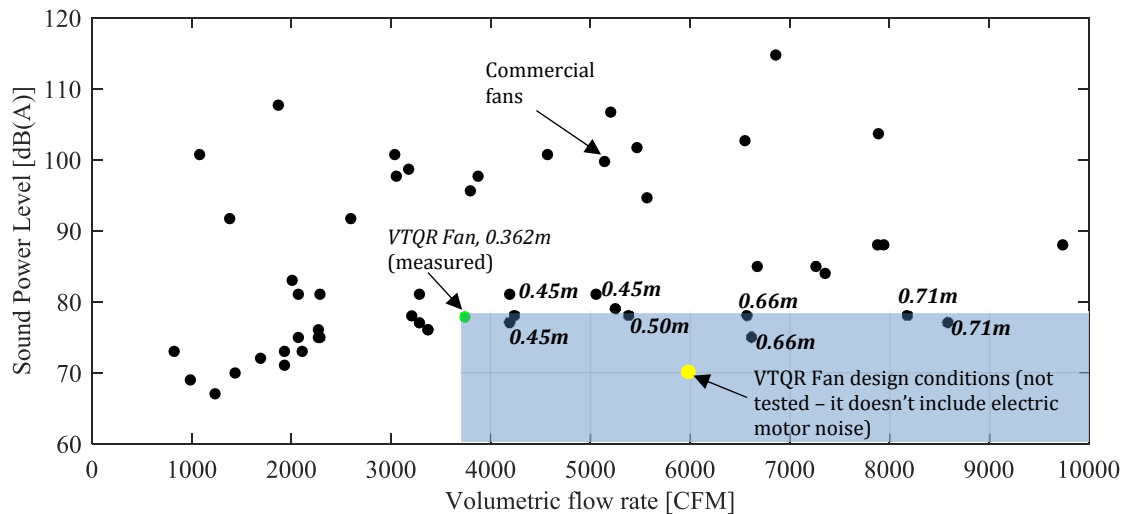
Figure 56: VTQR fan comparison to commercial ventilation fans.

4.2.2 Experimentally demonstrated VTQR rim-mounted approach
As discussed previously, the rim-driven and rim-mounted configurations had problems in terms of noise, electrical consumption, and durability. In spite of these issues, it was decided to test the VTQR fan also in the rim-mounted condition and compared to the free-tip configuration.

In Figure 57, the electrical power consumption of the fan rim-mounted configuration is compared to the fan free-tip configuration. As shown, the power consumption of the rim-mounted approach is significantly higher than the free-tip configuration. The main source of power consumption is the rolling resistance introduced by the O-rings (losses are due to deformation of the viscoelastic O-rings) used to

minimize metal to metal noise from the direct contact of the bearing and the aluminum ring. These losses make this implementation not yet practical unless this issue is further investigated and solved.

The fan sound power level spectrum in 1/3rd octave bands for the VTQR fan in both configurations at 1000 RPM is shown in Figure 58. The case of 1000 RPM was selected because this was the maximum speed that the rim-mounted fan attained. Although the rim mounted approach eliminated dominant sources of aerodynamic noise, it does introduce significant noise due to vibration of the duct, e.g. vibration induced by fan propagates through the 3 bearings and excites the duct. As shown in Figure 58, the rim-mounted approach increased the noise levels by 8 dB relative to the free tip configuration.

A positive result of the rim-mounted configuration was that the O-rings didn't fail or showed damage when the fan was operated for relatively long period of time (10-15 minutes). Thus, the mounting implemented in the VTQR fan showed improvement as compared to the subscale fan that failed in a minute or less of operation. However, more research is needed to fully address this issue.
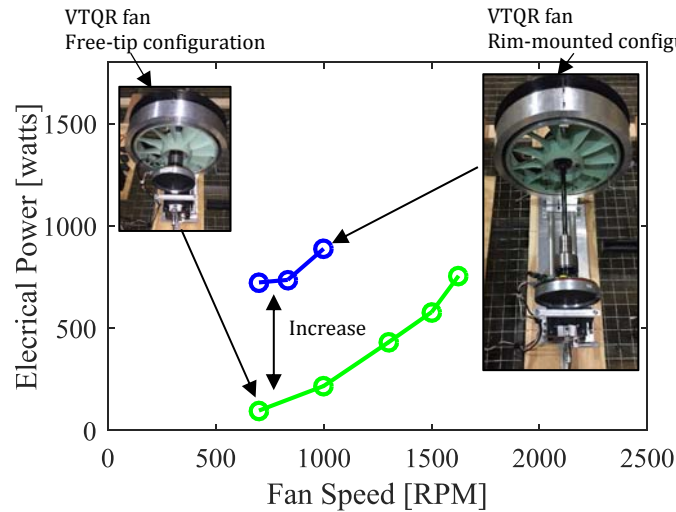
Figure 57: VTQR fan electrical power comparison between the rim-mounted and free-tip configurations.
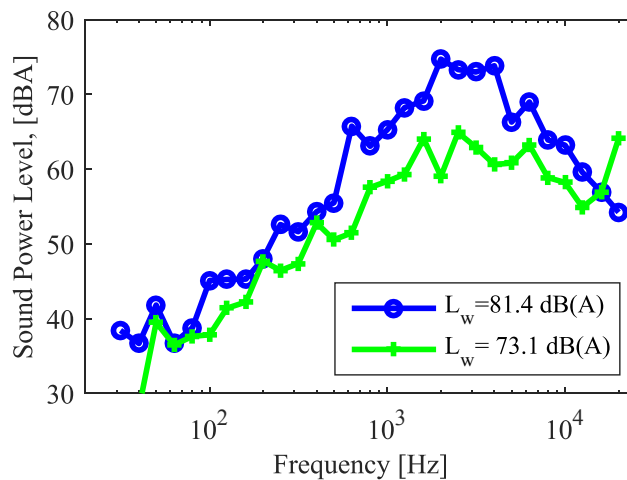
Figure 58: VTQR fan sound power level at 1000 RPM for the rim-mounted (blue) and free tip (green) configurations

4.2.3 Validated Aerodynamic Design of VTQR Fan

As it was the case for the subscale fans in Phase I, the aerodynamic predictions were also very accurate for the VTQR fan in Phase II. The accuracy of the predictions for this larger fan is demonstrated here by comparing measurements to predicted results.

Figure 59 shows the measured velocity profile for free tip configurations at a fan speed of 1616 RPM. The velocity profile for VTQR fan is compare to DFDC. As shown, the fan exit axial velocity is under predicted for inner 1/3rd of the blade span with an over prediction near the hub wall due to the blockage of the free-tip configuration. For the rest of the blade span, the predictions underestimate the measurements by about 4%. Unlike for the subscale fans in Phase I, in the Phase II a method was implemented to estimate the boundary layer as indicated in the figure. The results also show a relatively good prediction of the boundary layer. Figure 60 shows a comparison of the measured and predicted volumetric flow rate as a function of fan speed. As shown, the measurements show very good agreement with predictions, i.e. errors at 10% or less.

Finally, the measured and predicted fan mechanical power results for VTQR fan as a function of speed are shown in Figure 61. As illustrated, the measurements and predictions again agree very well.

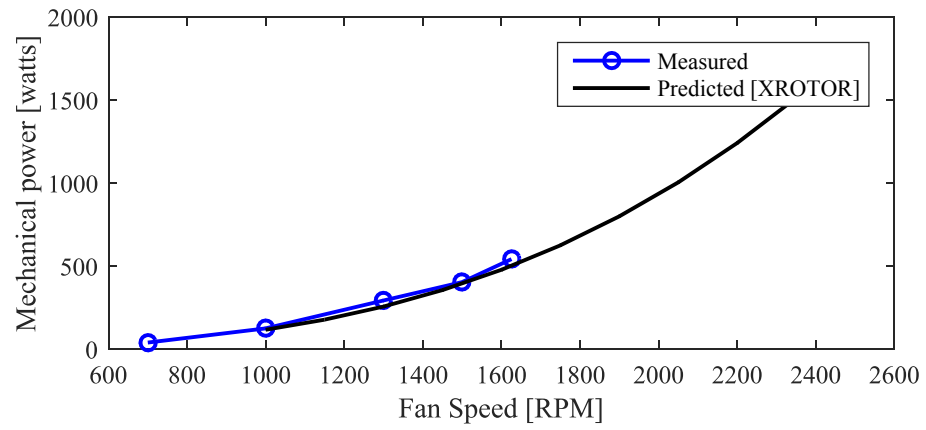The aerodynamic performance validations here and in section 4.1.3 demonstrates a high degree of confidence in the tools and design approached implemented in this project.
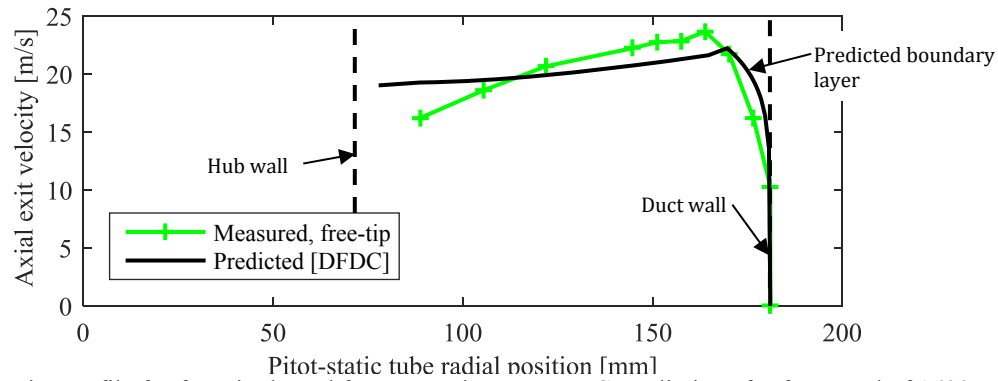
Figure 59: Velocity profile for free-tip ducted fan comparison to DFDC predictions for fan speed of 1600 RPM.
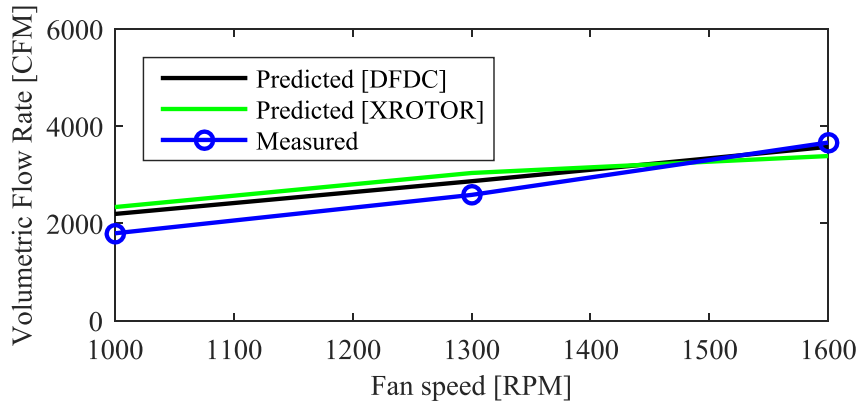
Figure 60: Fan volumetric flow rate vs fan speed for free-tip configuration.

44

Figure 61: VTQR fan mechanical power vs fan speed**.**

5. Publication Record and Dissemination Efforts:

The presentations and publications resulting from this research are listed below:

- **Conference presentation:** Hurtado, M., Wu, D., and Burdisso, R. (2017). *Design of low speed rim driven ventilation fan for minimum noise*, NOISE-CON 2017 Noise Control: Improving the Quality of Life, Grand Rapids, MI, June 12-14.

- **Conference presentation**: Hurtado, M., Wu, D., and Burdisso, R. (2017). *Quiet rim driven ventilation fan design*, 173rd Meeting of the Acoustical Society of America and the 8th Forum Acusticum, Boston, MA, June 25-29.

- **Conference presentation**: Hurtado, M., and Burdisso, R. (2018). *Design of a Low Speed Rim-Supported Fan for Minimum Noise,* FAN 2018: International Conference on Fan Noise, Aerodynamics, Applications and Systems, Darmstadt, Germany, April 18-20.

- **Conference presentation**: Hurtado, M., and Burdisso, R. (2018). *Low Speed Control Vortex Axial Fan Design for Minimum Noise,* INTER-NOISE 2018, the 47th International Congress and Exposition on Noise Control Engineering, Chicago, Illinois, USA, August 26-29 (abstract submitted).

- Hurtado, M., Wu, D., and Burdisso, R. (2018). *Design of low speed rim driven ventilation fan for minimum noise*, Noise Control Engineering Journal (in preparation).

6.   Conclusions and Impact Assessment:

This research effort significantly contributed to the improvement of the health and safety of mine workers by demonstrating the design of a quiet fan designed to reduce noise levels by 15-20dB while maintaining the same aerodynamic performance as commercial ventilation fans. The premise of this research effort was that a fan with a very low tip speed with an optimum blade design is the best approach to reduce noise. This is because the noise typically scales to the 4-6th power of the fan tip speed. The second premise to reduce noise was to implement a rim driven fan to eliminate many of the noise sources present in typical fans. To this end, the research approach was divided into two phases. In phase I, a small-scale fan demonstrator (0.134 m diameter) was used to provide an efficient approach to demonstrate and establish the benefits of the proposed technologies: lowering the fan tip speed and rim driven fan. In phase II, a quiet realistic fan (0.362 m diameter) was optimally designed to minimize noise using the lessons learned from the Phase I work.

In Phase I, two small scale fans were designed and tested showing excellent agreement with aerodynamic predictions. Consequently, validating the fan design process and the aerodynamic prediction tools. Furthermore, the two small scale fans were shown to have excellent aerodynamic properties that outperform over 80 commercial ventilation fans. Additionally, as part of phase I, four test rigs were designed and built. Key findings from rigs 1 through 4 indicated that the rim-driven fan concept cannot be successfully implemented with current technologies to achieve the project objectives. Additionally, key issues with the rim mounted approach were identified. The two main issues identified at the end of the Phase I effort were the noise levels (mainly mechanical) and the durability of the viscoelastic O-rings used in conjunction with miniature high speed bearings. Based on this key finding, the VTQR fan developed in Phase II was designed to be implemented as both rim-mounted and free-tip configurations.

In phase II, a new method to design quiet fans was developed. The new design method is characterized by a span wise changing axial velocity that ensures a higher flow rate contribution of the blade outer sections, i.e. axial flow increases from the blade hub to the tip. This allows for a higher volumetric flow rate at lower tip speeds and noise levels. Using this approach, a quiet realistic fan (0.362 m diameter) was optimally designed to outperform the baseline Cincinnati fan aerodynamically and acoustically. Proper design of the VTQR fan resulted in a compact, low tip speed fan with a high volumetric flow rate. The fan was fabricated and tested using a rim mounted and free-tip configurations. The rim mounted approach was found not to be practical with the current technology due to a significant increase in power consumption and noise. Consequently, the VTQR fan was tested using the free tip configuration. The VTQR fan was shown to outperform most commercial ventilation fans in terms of noise and/or CFM at the measured fan speed (64% of the design fan speed). The few commercial fans that are quieter and generate more CFM have dimeters that are between 25% and 100% larger than the VTQR fan, i.e. 0.45 to 0.71 m versus 0.362 m for the VTQR fan. ***Additionally, it has been demonstrated that an array of two VTQR fans operating at the measured speed (1616 RPM rather than the design speed of 2500 RPM) would generate the same volumetric flow rate as the baseline Cincinnati fan while reducing noise levels by 17.5 dB. Consequently, meeting the project objectives of same flow rate and noise level reduction of 15-20dB. Therefore, the implementation of the technologies demonstrated as part of this research effort can make portable ventilation fans one of the quietest sound sources in a mine operation.***

7. Recommendations for Future Work:

The obvious recommendation is the implementation of a DC brushless motor that has a higher efficiency and generates less noise. Consequently, a better motor can experimentally demonstrate that the VTQR fan can be quieter than what was achieved in this project, e.g. better that 15-20 dB A-weighted sound power level reduction relative to commercial fans. Another recommendation is to investigate the used of advanced blade designs. Specifically, the implementation of multi-blade technology has the potential to further reduce the fan speed and consequently the noise. It should be noted that there are no commercial fans using multi-element blades.

8. References:

[1] Bruneau, P. R. P. (1994). *The design of a single rotor axial flow fan for a cooling tower application*. Stellenbosch: University of Stellenbosch.

[2] Cherniack, M., Brammer, A., Cavallari, J., & Peterson, D. (2012, October 10). *Noise and Vibration Related Disease in the Mining*. Presentation to the Alpha Foundation for the Improvement of Mine Safety and Health, Inc. Charleston, West Virginia.

[3] Cincinnati Fan & Ventilator Co. (2016). *General Ventilation Products*. Retrieved from https://www.cincinnatifan.com/catalogs/GVP-1204-internet.pdf

[4] Cudina, M. (1992), *Noise generated by a vane-axial fan with inlet guide vanes*. Noise Control Engineering Journal,39(1), 21-30

[5] Davis, D. G. M. (1979). *The impact of noise regulations on propeller design* Dixon, S. L., and Hall, C. (2013*). Fluid Mechanics and Thermodynamics of Turbomachinery: Seventh Edition*,Elsevier Inc.

[6] Drela, M., & Youngren , H. (2005). *DFDC 0.70 [Online]*. Retrieved from http://web.mit.edu/drela/Public/web/dfdc/.

[7] Drela, M., & Youngren, H. (2011). *XROTOR [Online]*. Cambridge, MA: Massachusetts Institute of Technology. Retrieved from http://web.mit.edu/drela/Public/web/xrotor/

[8] Hurtado, M., Burdisso, R., and Wu, D. (2017). *Design of low speed rim driven ventilation fan for minimum noise*. Paper presented at NOISE-CON 2017 Noise Control: Improving the Quality of Life, June 12-14, Grand Rapids, MI., USA.

[9] Lawrence Berkeley National Laboratory. (1989). *Improving Fan System Performance, a source for industry*. The United States Department of Energy and Air Movement and Control Association International, Inc.

[10] Lee, H., Chung, S., & Hwang, S. (2008). *Noise source identification of a BLDC motor*. Journal of Mechanical Science and Technology, 22(4), 708-713.

[11] Matetic, R., Randolph, R., & Kovalchik, P. (2012). *Hearing Loss in the Mining Industry: The Evolution of NIOSH and Bureau of Mines Hearing Loss Research*.

[12] Mugridge, B., & Morfey, C. (1972). *Sources of noise in axial flow fans*. Journal of the Acoustical Society of America, 1411-27.

[13] Parzych, H. a.(1993). *Theory for noise of propellers in angular inflow with parametric studies and Experimental verification*. Retrieved from https://ntrs.nasa.gov/search.jsp?R=19930015905,

[14] Padhy, S. K. (1994). *Noise generation in small axial flow fans: analysis and some design guidelines for noise reduction*. Paper presented at the 45th Annual International Appliance Technical Conference Designs on Technology, 9-11 May 1994, Madison, WI, USA.

[15] Selig, M. S., Donovan, J. F., and Fraser, D. B. (1989). *Airfoils at low speeds*. Retrieved from Virginia Beach, Virginia.

[16] ThinGap, LLC. (2013). *Product Data Sheet*. Retrieved from http://www.thingap.com/wp content/themes/ndic/pdf/TG7140.pdf

[17] Vad, J., and Horvath, C. (2008). *The impact of the vortex design method on the stall behavior of axial flow fan And compressor rotors*. Paper presented at the 2008 ASME Turbo Expo, June 9, 2008 - June 13, 2008, Berlin, Germany.

[18] Vad, J., and Bencze, F.(1998). *Three-dimensional flow in axial flow fans of non-free vortex design*. International Journal of Heat and Fluid Flow, 19(6), 601-607.

9. Appendices:

9.1 Appendix A: Motor selection

The DC Brushless motor used for driving the fan demonstrators in phase I and II of this research effort is the model TG7140 ThinGap motor. The motor was selected because it allows testing of the small scale fans up to 8100 RPM in a rim driven configuration. With a power density of 4.51 kW/kg, the 0.854 kg Thingap motor is able to generate up to 4.52 N-m (3.33 lbf-ft), well past the design power and torque of the small scale fans. Using a gearbox with a ratio of 3, the nominal torque can be increased to 13.52 N-m at a maximum speed of 2713RPM which is sufficient to drive a large fan. Other motors were also considered for this research. However, the ThinGap TG7140 is superior in terms of its performance as shown in Figure 62. Here the performance of the ThinGap TG7140 motor is compared to other ring motors fabricated by Applimotion Inc. at the maximum continuous operating speed. This figure shows the motor torque, mechanical power, and electrical power as a function of motor tip speed (rpm) for the ThinGap motor (continuous curves) and the Applimotion UTS series motors (markers) at the maximum operating speed. The results shown in this figure were obtained by developing a numerical model using parameters from the company datasheets. The figure indicates that the ThinGap TG7140 has significant higher speed and torque range than the Applimotion motors. Thus, it was confirmed that the ThinGap motor was the best option for the project. The ThinGap TG7140 motor assembly and its mounting system is shown in Figure 63. As illustrated, the ThinGap TG7140 motor assembly consists of three major parts: stator, rotor, and mounting system, and they are highlighted in cyan, green, and yellow respectively in Figure 63. The stator has all the electrical components attached to it, including 3 hall-effect sensors, a thermal sensor, a controller connector, and the power supply. Its mounting system has a shaft and a bearing clamped at the center.
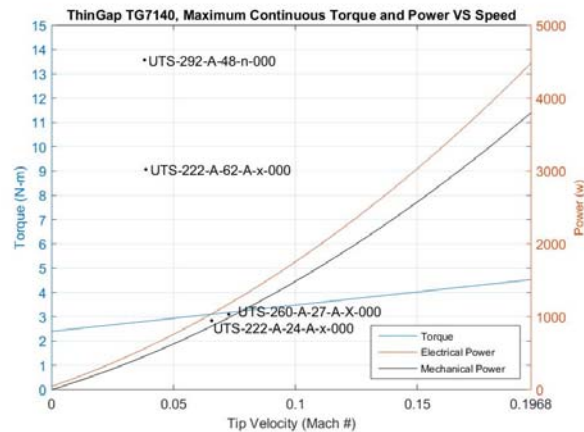
Figure 62: Comparison of ThinGap TG7140 and Applimotion motors performances at maximum continuous operating speed.
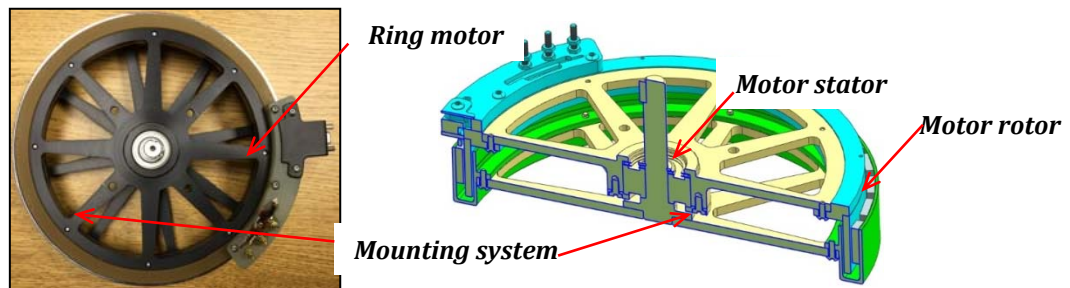
Figure 63: ThinGap TG7140 motor with the ThinGap mounting system.

9.2 **Appendix B: Codes used for Design**

The following sections present the codes used in this research effort.

XROTOR

XROTOR is an open source software developed by Mark Drela and Harold Youngren at MIT in the 1980's for the design and analysis of ducted and free-tip propellers, and windmills. XROTOR is composed of a collection of menu-driven routines which uses the Betz-Prandlt approach or a Goldstein approach to calculate the incoming and induced velocities by numerically solving for the exact perturbation potential flow field about the helical vortex sheet wake. XROTOR requires sensible starting conditions for convergence and uses the first derivatives of the parameters to calculate the change for the new iteration using the newton method. Therefore, the design parameters required by XROTOR to design a rotor are the airfoil polars, tip radius, hub radius, hub wake displacement radius, airspeed, rpm or advance ratio, thrust or power and the lift coefficient. XROTOR is also able to analyze the rotor at off-design conditions by calculating the off-design operating points for a sequence of RPMs.

DFDC

To assess the fan performance incorporating the duct-hub effects, the analysis has been conducted using the code DFDC (Drela and Youngren, 2005). This code models the fan with any arbitrary duct-hub shape. The only limitation is that the ducted rotor has to be axisymmetric. DFDC combines a lifting line representation of the rotor with an axisymmetric panel representation of the duct and hub to compute the self-induced velocities form the fan, duct, and center body. Furthermore, DFDC accounts for losses due to non-uniform loading of the ducted flow field.

Mugridge-Morfey

The Mugridge-Morfey method is a first principle/empirical model to predict the self-noise generated by the turbulence over the rotor (airfoil trailing edge noise) including the effect of the tip gap source. The model predicts the noise due to boundary layer pressure fluctuations interacting with the trailing edge (Sharland, 1964; Mugridge, 1973; Gliebe , 2002). The effect of the tip gap is included in the model. The method gives an expression relating the fan broadband acoustic power to key parameters of the fan such as chord, blade planform, number of blades, inlet Mach number, and airfoil drag and lift coefficients. Because it is computationally efficient, this code is ideally suited for trade studies.

WOBBLE

Wobble is a frequency domain code for rotor alone tonal noise prediction and it has been successfully validated in the open literature (Hanson and Parzych, 1993). The code computes the tone noise associated with subsonic propellers and axial fans with varying inflow angle and predicts the axial and circumferential directivity in the near and far-fields. The acoustic model accounts for all unsteady sources such as thickness and surface loading effects from the blades which are, respectively, the monopole and dipole sources in the Ffowcs Williams and Hawkins (1969) inhomogeneous wave equation. In subsonic flow, the contribution of the quadrupole term (due to turbulence) is normally negligible compared to the other two and thus not predicted by WOBBLE. As documented by Goldstein (1979), a set of sources (monopoles and dipoles) is distributed over the blades surface using strip theory. The source terms are determined from the pressure distribution over the blades, e.g. such as that obtained from XROTOR or a CFD calculation. The radiation into the near and far-field is predicted using Goldstein's acoustic analogy or the Ffowcs-Williams and Hawkings equation modified to account for a moving medium.

9.3 Appendix C: Characteristic of Commercial Ventilation Fans

The data of commercial ventilation fans has been collected from various well-known manufacturers. These companies have well-established datasheets that are available on their official websites. These datasheets have hundreds of fan models with different sizes and configurations, but only axial electrical-driven fans are considered in this investigation. Figure 64 shows examples of axial fans from Nicotra Gebhardt. For the design purpose of temporarily mounted fans, this investigation only includes fan diameter ranging from 300mm to 720mm.

(a)   (b)

Figure 64: Nicotra Gebhardt axial fans (a) Model: ARA61 (b) Model: ARA62.

The specifications of 80 axial fans are presented in this Appendix in graphical form. The data includes fan diameter, number of blades, revolution per minute (rpm), volumetric flow rate (cubic feet per minute, cfm), and sound pressure level (if available in the datasheets). Figure 65 shows the fan diameter against cfm. This figure indicates that fan blade diameter is proportional to the volume flow rate. Figure 66 and Figure 67 show volumetric flow rate (CFM) and sound pressure level against operational speed (RPM). It is important to note that sound pressure level measurements are taken from different distances based on the manufactures datasheets.
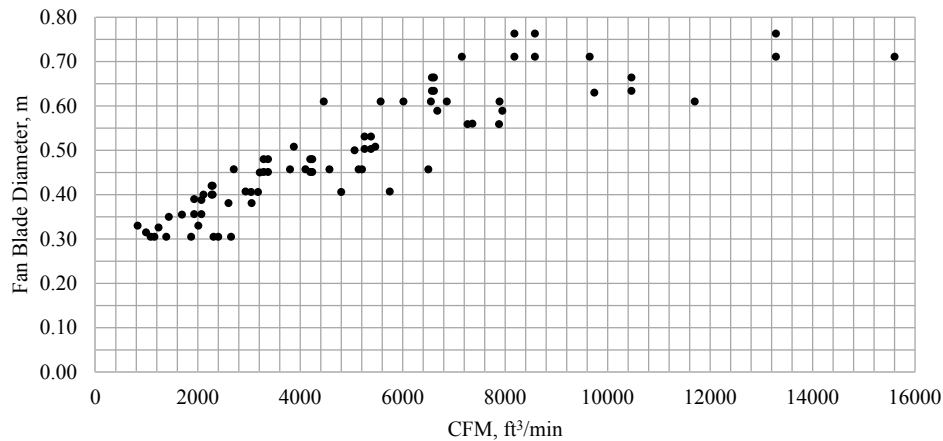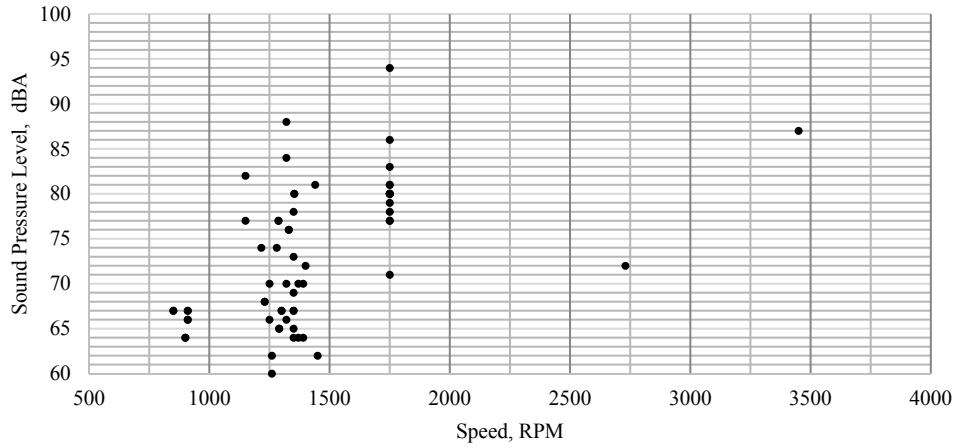

Figure 65: Fan size vs. Volume flow rate.
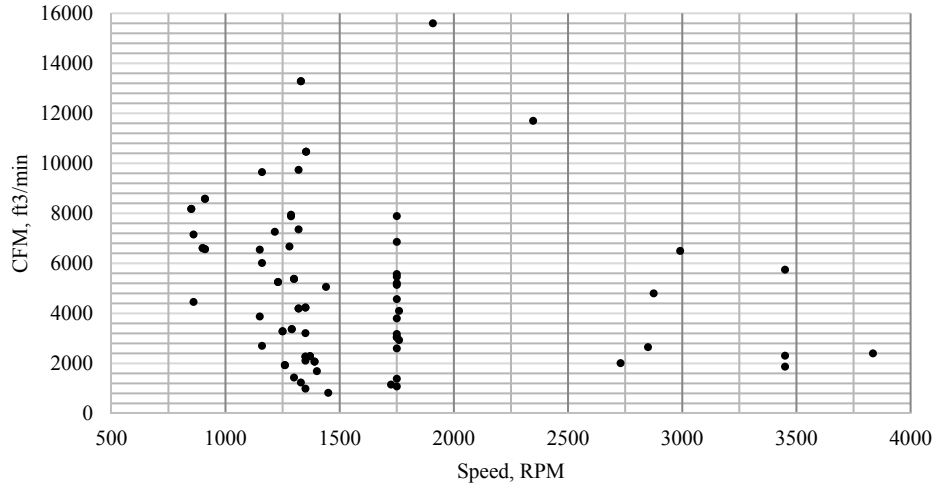
Figure 66: Volume flow rate vs. fan operational speed.

Figure 67: Sound pressure level against fan operational speed.

As illustrated in Figure 66, Figure 67, and Figure 68, it is difficult to compare and identify design trends when fans are of different sizes. Consequently, it is important to normalize the data to extract useful information for design and comparison purposes. The key fan parameters that were normalized are:

- The volumetric flow rate (cfm)
- The fan speed (RPM)
- The sound pressure level (dB)

The volumetric flow rate ($\dot{V}$) was normalized by the fan area to give the exit flow velocity (V_{exit}) as

$$V_{exit} = \frac{\dot{V}}{A} \qquad \textbf{(9.1)}$$

Where $A = \pi \left(\dfrac{D}{2} \right)^2$ is the cross sectional are of the duct (m^2)

D is the fan diameter of the fan blade (m)

53

The fan speed was normalized by the fan diameter resulting in the fan tip velocity, expressed in Mach as

$$M_{Tip} = \frac{\pi D \omega}{60 * c}$$ (9.2)

Where c is sound speed at standard sea level (343.2 $m/\sec$)
              D is diameter of the fan blade (m)
              ω is angular velocity (RPM)
              V_{Tip} is the blade tip speed (m/s)
              M_{Tip} is tip speed in terms of Mach number

The sound pressure level reported at a given distance was used to estimate the sound power level produce by the fan, which it is independent of distance. Assuming spherical waves, the sound power level was computed as

$$L_W = L_P(R) + 10 Log_{10}(4\pi R^2) = 10 Log_{10}\left(\frac{W}{W_{ref}}\right)$$ (9.3)

where L_W is source sound power level (dB)

           L_P is sound pressure level provided by manufacturers at distance, R (dB)

           W is sound power at the source (watts)

           W_{ref} is reference sound power (10^{-12} watts).

However, the sound power level does not account for the size of the fans. Consequently, to account for the different size of the fans the average sound intensity level was computed. The sound intensity level is the sound power level radiated per unit area. In this case, the area used to compute intensity is twice the duct area which corresponds to the duct inlet and outlet. The expression relating sound power level $L_W(dB)$, sound intensity level $L_I(dB)$, and fan diameter d is:

$$L_W(dB) = L_I(dB) + 10\ Log_{10}\left(\frac{\pi d^2 \times 2}{4}\right)$$ (9.4)

Therefore the sound intensity level can be computed as

$$L_I(dB) = L_W(dB) - 10\ Log_{10}\left(\frac{\pi d^2 \times 2}{4}\right)$$ (9.5)

The normalized data charts used in this work are shown and described next. Figure 88 shows the axial ventilation fans' exit velocity (V_{exit}) versus fan tip velocity. This clearly shows the trend that a higher tip velocity leads to higher exit velocity (almost linear relationship).
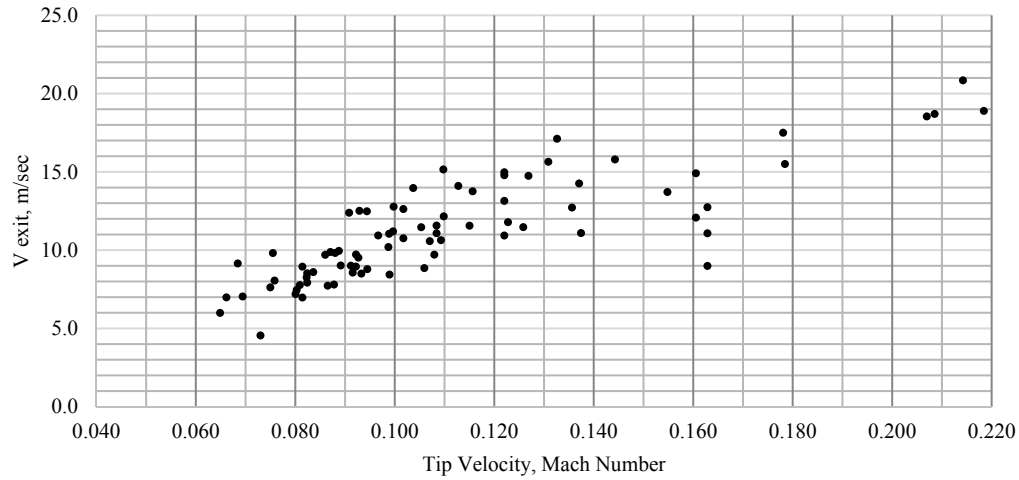
Figure 68: Normalized plot of flow exit velocity against tip velocity.

Figure 69 shows the sound intensity level for the commercial fans as a function of tip Mach number. It can be observed that the noise levels increase significantly with the fan tip speed, as expected. Consequently, it can be observed that there is a trade-off between aerodynamic performance and noise.
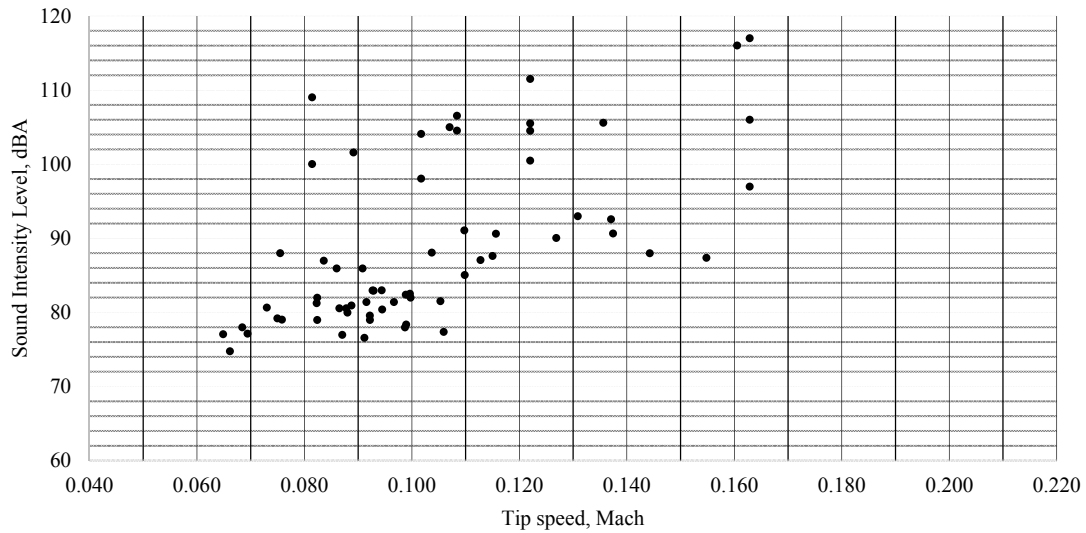

Figure 69: Fan overall A-weighed sound intensity level vs fan tip velocity.

9.4   Appendix D: Motor noise reduction

As part of this research effort, efforts were dedicated to identifying motor noise sources in test rig 4 and reducing them. To this end, noise measurements of the motor alone were performed at several RPMs. However, the case of 4000 rpm will be used to describe the findings of this effort.

Figure 70 shows the narrowband sound power spectrum for the motor alone at 4000 rpm. This plot shows a number of unique features. They are:

- There is a very dominant noise feature at 20,000 Hz that is clearly associated with the switching frequency driving the motor windings. This noise is typical of brushless motor.
- There are two "hey-stacks" at ~1000 and 2500 Hz. These features are typical of vortex shedding type of noise sources.
- The peak at 70 Hz has the classical shape of a lightly damped structural resonance.
- There are many pure tones over the frequency range 2000 to 10000 Hz. These tones are also typical of brushless motors. They are produced by non-uniform (vary with respect to the rotor angular position) electromagnetic forces in the airgap between the stator and rotor. These unbalanced forces are transmitted to the motor rotor causing vibration and noise (Lee et.al., 2008).
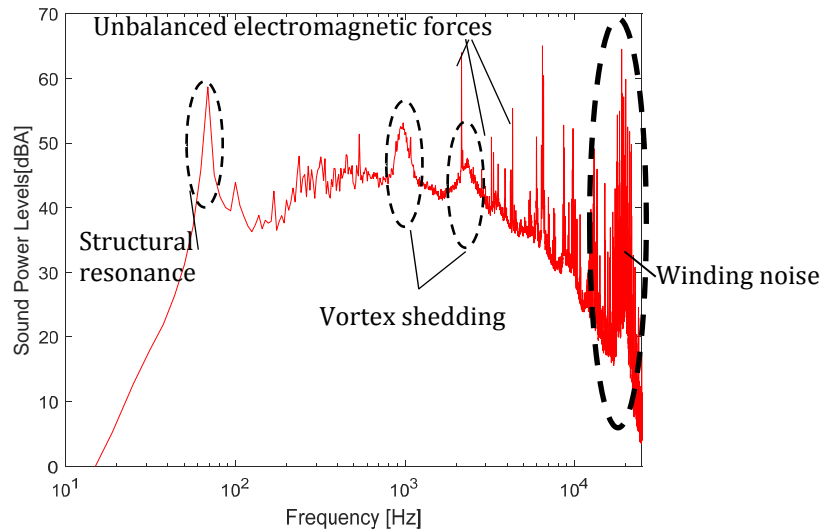
Figure 70: Narrowband A-weighed sound power spectrum for motor alone at 4000 rpm.

Since the motor itself generates noise, several noise reduction methods were attempted. The results of these efforts are summarized in Table 12. As observed, the motor itself without any treatment generates approximately 76.5 dBA at 4000 RPM (Table 12a).

The first effort was to reduce the "hey-stacks" in the spectrum. It was assumed that these were generated by potential vortex shedding from the open frame of the rotor. Using aluminum tape the open frame was closed essentially resulting in a solid disk as shown in Table 12b. Figure 71 compares the narrowband spectrum of the motor only with the motor with the treatment to eliminate the vortex shedding from the open frame of the rotor. It is clear that the vortex shedding at ~ 1000 Hz was completely eliminated (~15 dB of reduction at 1000Hz). As shown in Table 12b, an overall reduction of 2.8 dB was achieved.
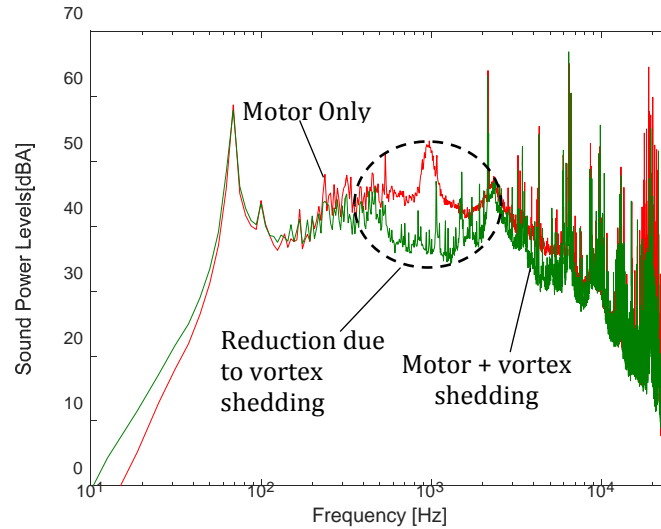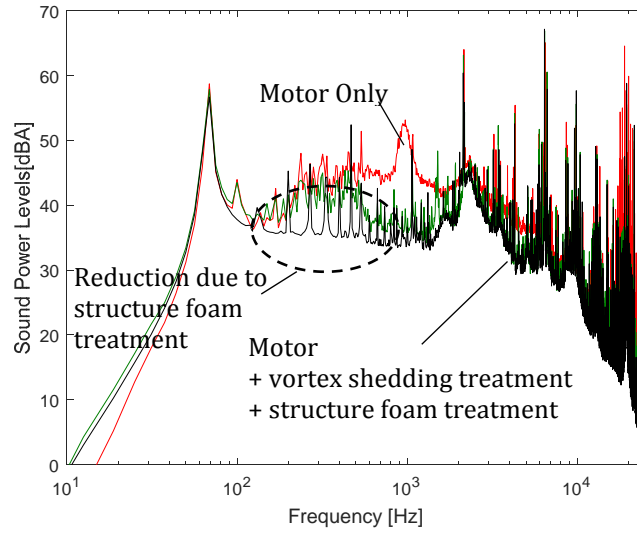
Figure 71: Attenuation due to elimination of the vortex shedding from the open frame of the rotor.

Significant vibration of the test rig support structure was observed. This structure is excited by the motor vibration. For this reason, the structure was covered with open cell foam as shown in Table 12c. The resulting spectrum from covering the support structure with foam plus the vortex shedding treatment is shown in Figure 72. To identify the effectiveness of the treatment, the spectrum for case "a" (motor alone) and case "b" (motor alone + vortex shedding treatment) are also included in this figure. It is clear that significant noise reduction was obtained in the 125 to 1000 Hz frequency range. Relative to the motor alone case, the overall noise reduction is now 3.5 dB.

To further reduce the noise levels, the motor was also covered with open cell foam of ~ 2" thickness as shown in Table 12d. Figure 73 shows the spectrum together with all the results from Figure 72. It is very clear that significant noise reduction was obtained at frequencies above 1250 Hz. Relative to the motor alone case, the noise reduction with all 3 treatments is now 10.5 dB lower (Table 12d).

For the sake of clarity, Figure 74 shows the spectrum for the motor alone and with all treatments. It is clear that that there are some dominant noise components that still need to be reduced. Thus, future work should be focused on further reducing the motor noise. One such treatment is the reduction of the vortex shedding at 2500 Hz. We believe that this noise is due to vortex shedding produced by the array of 32 magnets on the rotor. This can be observed in Figure 74. Another treatment would be to replace the simple foam around the motor for a better designed "enclosure" that includes a hard surface (plastic) with foam inside. We also believe that the strong resonance at 70Hz is a structural resonance of the test rig support structure.

Figure 72: Attenuation due to covering the structure with foam (results from Figure 71 also included).
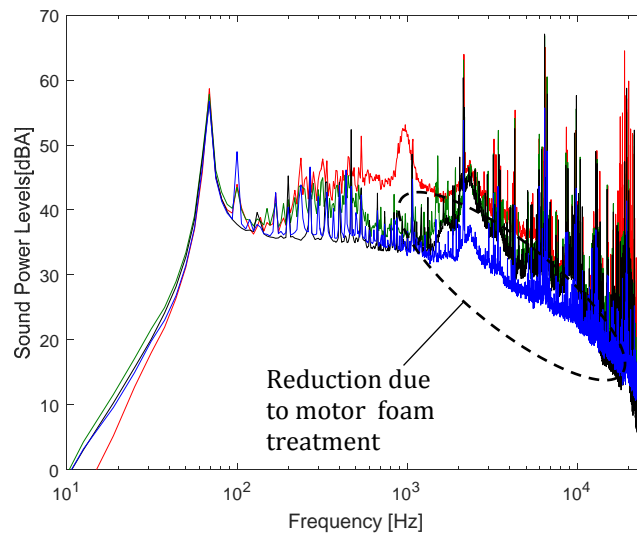
Figure 73: Attenuation due to covering the motor with foam (results from Figure 72 also included).
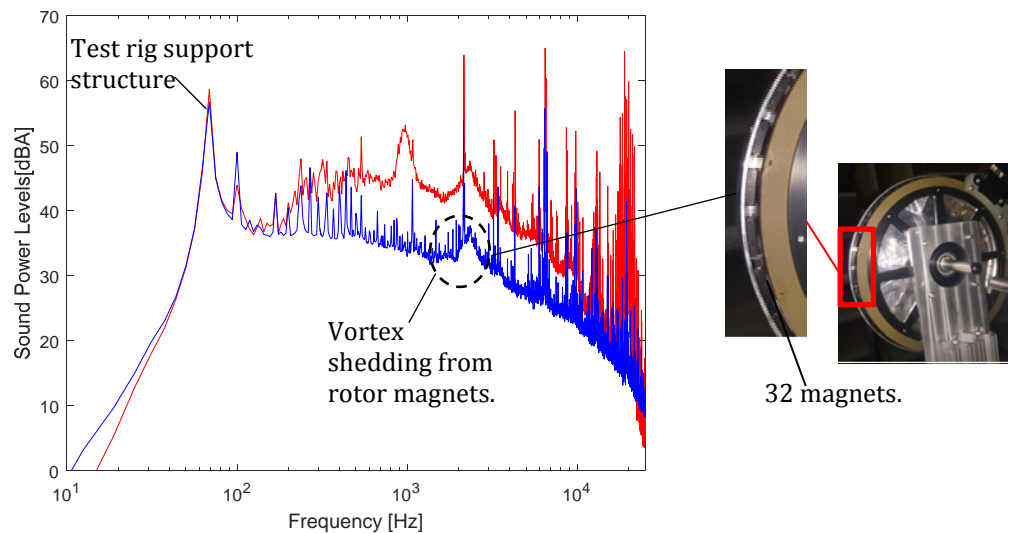
Figure 74: Attenuation of motor noise due all treatments.

Table 12: Motor and test rig 4 noise reduction methods.

Test description	Test set up	Overall sound power level at 4000 RPM
a) Motor only		76.5 dBA
b) Motor + vortex shedding treatment		73.7 dBA
c) Motor + vortex shedding treatment + structure foam treatment		73.0 dBA
d) Motor + vortex shedding treatment + structure foam treatment + motor foam treatment		66.0 dBA